EVALUATION OF CO_2 SEQUESTRATION THROUGH ENHANCED OIL RECOVERY IN WEST SAK RESERVOIR

By

Vahid Nourpour Aghbash

RECOMMENDED:

Advisory Committee Member

Advisory Committee Member

Mahboobat Ahmadi

Advisory Committee Chair

Chair, Department of Petroleum Engineering

APPROVED:

Charles E Mayer

Dean, College of Engineering and Mines

John P Eichelberger

Dean of the Graduate School

29 April 2013

Date

EVALUATION OF CO_2 SEQUESTRATION THROUGH ENHANCED OIL RECOVERY IN WEST SAK RESERVOIR

A

THESIS

Presented to the Faculty

of the University of Alaska Fairbanks

in Partial Fulfillment of the Requirements

for the Degree of

MASTER OF SCIENCE

By

Vahid Nourpour Aghbash

Fairbanks, Alaska

May 2013

Abstract

CO_2 enhanced oil recovery (EOR) has been proposed as a method of sequestering CO_2. This study evaluates using CO_2 as an EOR agent in the West Sak reservoir. The injected CO_2 mixes with the oil and reduces the oil viscosity, enhancing its recovery. A considerable amount of CO_2 is left in the reservoir and 'sequestered'. Due to low reservoir temperature, this process can lead to formation of three hydrocarbon phases in the reservoir. An equation of state was tuned to simulate the West Sak oil and complex phase behavior of the CO_2-oil mixtures. A compositional simulator capable of handling three-phase flash calculation and four-phase flow was used to simulate CO_2 injection into a three-dimensional heterogeneous pattern model.

The results showed that CO_2 EOR in the West Sak reservoir increases oil recovery by 4.5% of original oil in place and 48 million metric tons of CO_2 could be sequestered. Ignoring four-phase flow underestimated oil recovery and sequestered CO_2 volume, enriching the CO_2 with natural gas liquid decreased sequestered CO_2 volume without a significant increase in oil recovery. Dissolution of CO_2 in the water phase and different water/CO_2 slug sizes and ratios did not change the sequestered CO_2 volume and oil recovery.

Table of Contents

List of Figures

Page

List of Tables

Page

Acknowledgments

This project was funded by the USAF Office of Scientific Research, award no. FA9550-11-1-0006.

My special gratitude goes to Dr. Ahmadi, my thesis committee chairman and advisor, for his support, background knowledge and guidance during the course of this work. I also would like to acknowledge my committee members, Dr. Hanks and Dr. Dandekar, for their feedback, help and support.

I would like to extend my gratitude to the students, faculty and staff members of the Petroleum Engineering Department of the University of Alaska Fairbanks.

I would like to acknowledge Dr. Sepehrnoori at the Center for Petroleum and Geosciences Engineering at the University of Texas Austin for providing the simulator, UTCOMP. I also would like to thank Dr. Kalaei for his guidance and help.

My deepest thanks go to my family for their support and encouragement during this program, as well as throughout my entire life.

Chapter One: Introduction

1.1 Overview

Concentration of greenhouse gases (GHGs) in the atmosphere has increased since the industrial revolution (EPA, 2012). This increase has amplified the greenhouse effect and is very likely responsible for global warming (EPA, 2012).

Carbon dioxide (CO_2) was responsible for 83.6% of total U.S. GHG emissions in 2010 (EPA, 2012). Atmospheric CO_2 concentration increased by 39% between 1750 and 2010 (EPA, 2012). Carbon dioxide is a byproduct of fossil fuel combustion, which satisfies approximately 82% of energy demands in the U.S. and the world (EIA, 2012a, b). Projections show that the contribution by non-CO_2 emitting energy sources will not significantly increase until 2035 and, until then, that fossil fuels will hold their share in the world energy supply (DOE/EIA, 2012). During this time, CO_2 emissions will increase by an estimated 2% (DOE/EIA, 2012), increasing the atmospheric CO_2 concentration and amplifying the greenhouse effect. This could yield a rise in global temperature and cause catastrophic climate change. Decreasing the atmospheric CO_2 concentration could prevent or mitigate these potential consequences.

Reducing CO_2 emissions and carbon capture and sequestration are the possible options to decrease CO_2 concentration. Using more efficient fuels or renewable energy sources decreases CO_2 sources and emissions; however, economical, technical and environmental issues prevent large-scale implementation of renewable energy projects. Forestation decreases atmospheric CO_2 by the photosynthesis process; however, the process is slow, and large-scale planting of trees requires vast areas. With CO_2 sequestration, CO_2 is captured from the source/atmosphere and disposed permanently (Bachu, 2000). Figure 1 shows a sequestration system diagram. It is a medium-term solution for decreasing atmospheric CO_2 concentration and reducing climate change effects. It also makes it possible to continue current fossil fuel usage while renewable technology is being developed (Gaspar et al., 2005).

Different methods are proposed for CO_2 sequestration (Bachu, 2000). Oceans provide the largest potential sink for CO_2 sequestration (IEA, 2002). However, technical, environmental and legal issues prevent this approach.

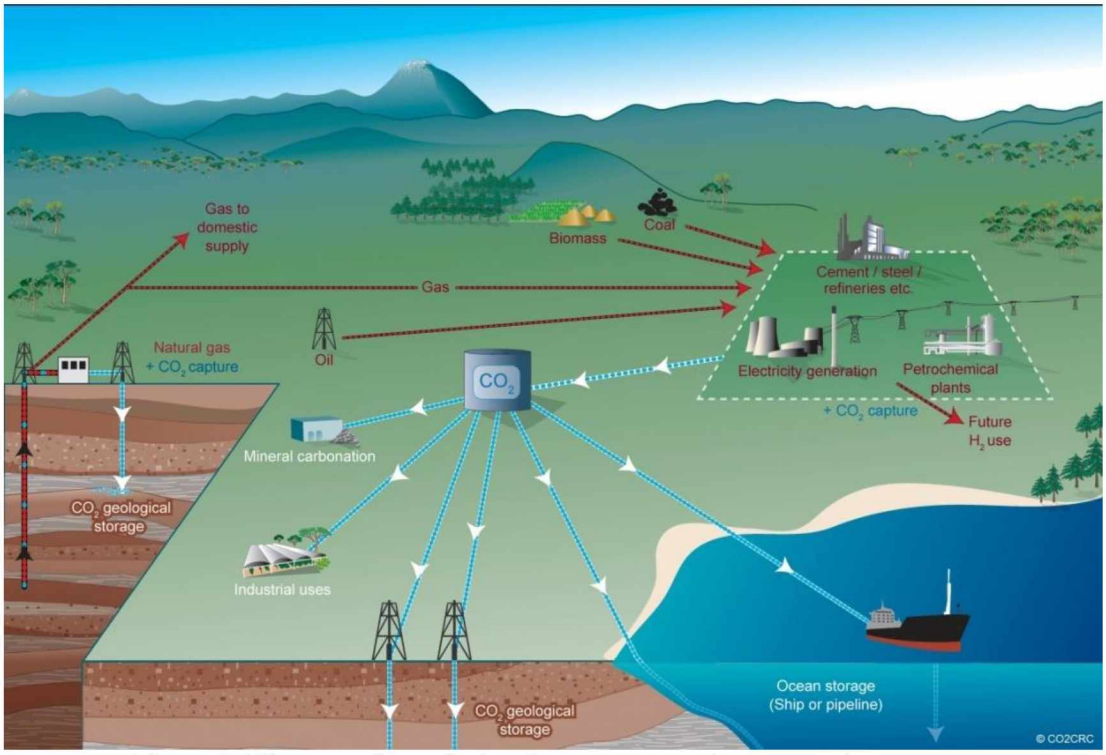

Figure 1: Diagram of a typical carbon capture and sequestration system (CO2CRC Images and Videos, 2012)

Geological sequestration is the safest and most attractive method for long-term sequestration due to a well-understood mechanism and developed technology. The main geologic techniques suggested to be most suitable for CO_2 storage (Bachu, 2000) are:

1. Injection into deep saline aquifers;
2. Using CO_2 as an enhanced oil recovery (EOR) agent in a mature oil field;
3. Injection into depleted oil and gas reservoirs;
4. Injection of CO_2 into deep coal beds to recover methane;
5. Injection into salt caverns; and
6. Injection into mafic and ultramafic rocks.

The major challenge for wide-scale implementation of geological CO_2 sequestration projects is the high cost of the process. The CO_2 must be captured, transported, compressed and then injected. Injecting CO_2 as an EOR agent increases oil recovery and can compensate for some of the CO_2 capture and sequestration costs. The mechanisms of enhanced oil recovery by CO_2 are well studied, and CO_2 injection technology is well developed. The existing reservoir demonstrates the integrity of the cap rock and availability of pore volume for sequestration. Available reservoir characterization data and operational infrastructure can further decrease project costs (Bachu, 2000).

Injection of CO_2 into viscous and heavy oil reservoirs has been evaluated and implemented in different fields, such as Bati Raman field in Turkey (Sahin et al., 2008), and Wilmington field in California, U.S. (Saner and Patton, 1986). The Alaska North Slope (ANS) holds an immense volume of viscous and heavy oil. Injection of CO_2 has the potential of increasing oil recovery from these immense reservoirs while sequestering a considerable amount of CO_2. Increased oil recovery can compensate for the cost of CO_2 capture and transport.

1.2 Objective

This thesis presents a study of CO_2 sequestration in the West Sak reservoir. In shallow reservoirs such as the West Sak reservoir where temperatures are below 120°F, the mixture of CO_2 and oil forms a complex multi-liquid phase equilibrium (e.g., separate HC-rich and CO_2-rich liquid phases). Previous studies of CO_2 injection in the West Sak reservoir did not consider this complex phase behavior. This study evaluates CO_2 injection in the West Sak reservoir while capturing this complex phase behavior in order to:

1. Estimate increased oil recovery due to CO_2 injection
2. Quantify sequestered CO_2 volume
3. Study the effect of (a) ignoring CO_2-oil complex phase behavior; (b) enriching CO_2 with NGL; and (c) CO_2 dissolution in water.

Chapter Two: Literature Review

2.1 Description of West Sak Reservoir

An estimated 15 to 25 billion barrels of viscous and heavy oil is trapped in the shallow pools of the Alaska North Slope (ANS) (Panda et al., 1989). The majority of this oil resides in West Sak and Schrader Bluff Formations in the Kuparuk River Unit (KRU), Milne Point Unit (MPU), Nikaitchuq, and the western Prudhoe Bay Unit. The West Sak reservoir in KRU, shown in Figure 2, contains 7 to 9 billion barrels of original oil in place (OOIP) (McGuire et al., 2005).

The West Sak reservoir stratigraphy is the stratigraphic equivalent of the Schrader Bluff Formation seen in MPU, Nikaitchuq, and western Prudhoe Bay. The West Sak reservoir consist of inner shelf to shallow marine or delta front sands of, Late Cretaceous age. The reservoir interval consists of very fine- to fine-grain unconsolidated sandstones separated by layers of siltstone and mudstone (Werner, 1987). The poor consolidation causes a large amount of sand production that challenges the efficiency of oil production.

Two distinctive members, Upper and Lower West Sak, divide the West Sak interval (Werner, 1987). The Upper West Sak consists of two sand packages, sands D and B, each 25 to 40 ft thick. The Lower West Sak has one main sand package, sand A, that consists of 10 ft thick amalgamated sand units made up of thin-bedded sand layers (0.2–5 ft) and interbedded siltstone and mudstone. Gross thickness of the West Sak reservoir is about 700 ft in the southwest area of KRU. It decreases to 350 ft in the northeast area, making the average gross thickness 450 ft (Werner, 1987). Net pay thickness of the reservoir interval is about 90 ft (Targac et al., 2005). The reservoir interval lies between 2400 ft subsea true vertical depth (SSTVD) in western areas of KRU and 3800 ft SSTVD in eastern areas.

Permafrost extends to about 1600 ft SSTVD in the ANS area. Due to proximity of the permafrost, reservoir temperature is relatively low, 45 to 100°F depending on depth.

Low reservoir temperature and oil degradation in shallow parts of the reservoir make the oil very viscous (>300 cp). This high viscosity increases the difficulties associated with oil production. Therefore, operators designated the eastern and deeper part of the reservoir as the West Sak Core Area (WSCA), shown in Figure 3. This core area contains an estimated 2.5 billion barrels of OOIP with viscosity of 20 to 100 cp at reservoir initial pressure and temperature of 1600 psia and 75°F.

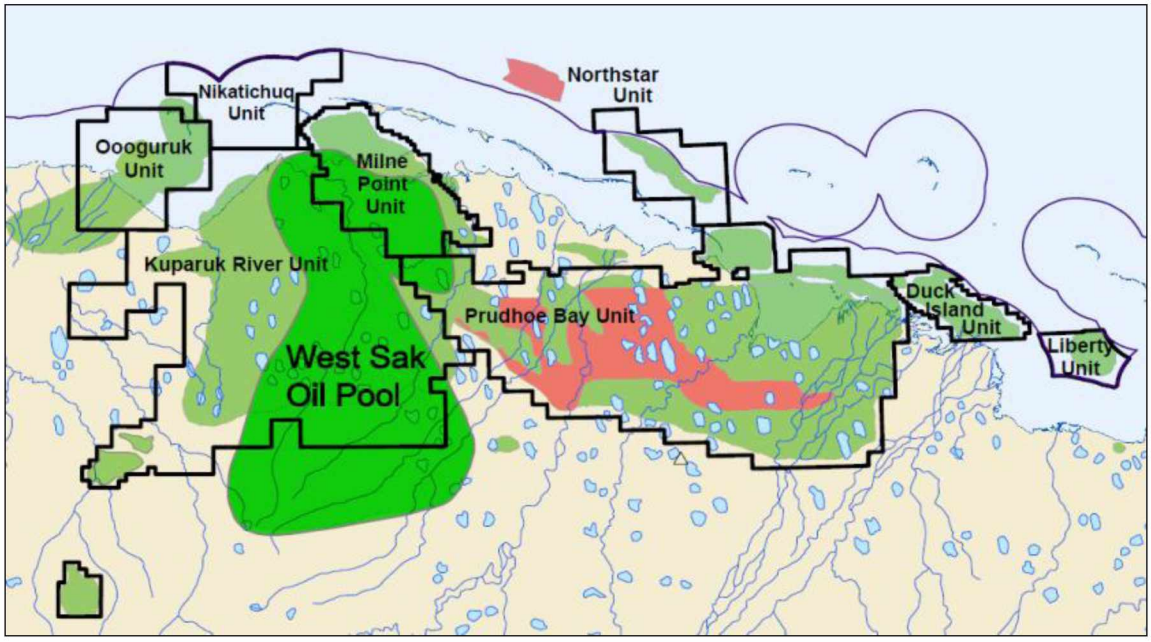

Figure 2: Map of West Sak reservoir in ANS (AOGCC Pool Statistics, 2004)

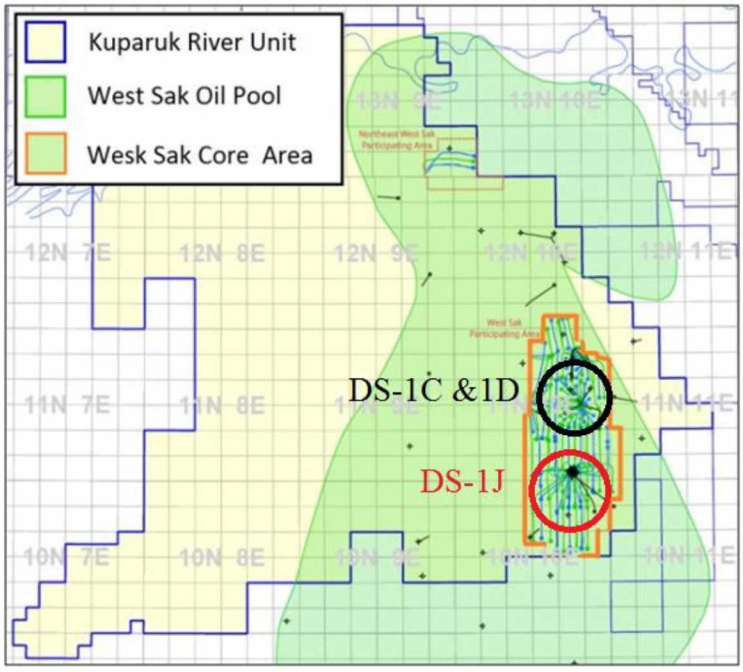

Figure 3: Location of West Sak Core Area (modified from AOGCC Pool Statistics, 2004)

2.2 West Sak Development

Targac et al. (2005) provided a comprehensive description of the West Sak development. Here is a summary of it:

A pilot project in the West Sak KRU reservoir started in the 1980s, a decade after the reservoir's discovery in 1971. The project was implemented in the DS-1J area of the reservoir, due to its better oil quality. Fifteen vertical wells were drilled in an inverted nine-spot pattern with five-acre well spacing to inject water and produce oil from all three major West Sak sand packages: A, B, and D. During the first two years, considerable rock and fluid information was gathered and 900,000 barrels of oil was produced. This pilot project confirmed that oil production is practical using tightly spaced waterflooding.

The second phase of development started in 1997. To decrease project cost, the DS-1D area was chosen due to availability of in-site infrastructure. The project used a similar well pattern; however, the well spacing was increased from 5 to 40 acres. Because of a low oil production rate, results were only marginally economic.

Horizontal and multilateral production wells were implemented in 1999 to boost the oil production rate. Lateral length of horizontal and multilateral wells increased from 2000 ft to over 6000 ft. This change increased oil recovery per well and decreased production cost. Horizontal injectors were also drilled in 2002.

Initially, development was limited to sands D and B. Sand A was added to the development plan, but sand production problems initiated afterward. After evaluation of different well designs, dedicated laterals to sands D and B and an undulating lateral in sand A2 were determined to be the optimum well design (Figure 4).

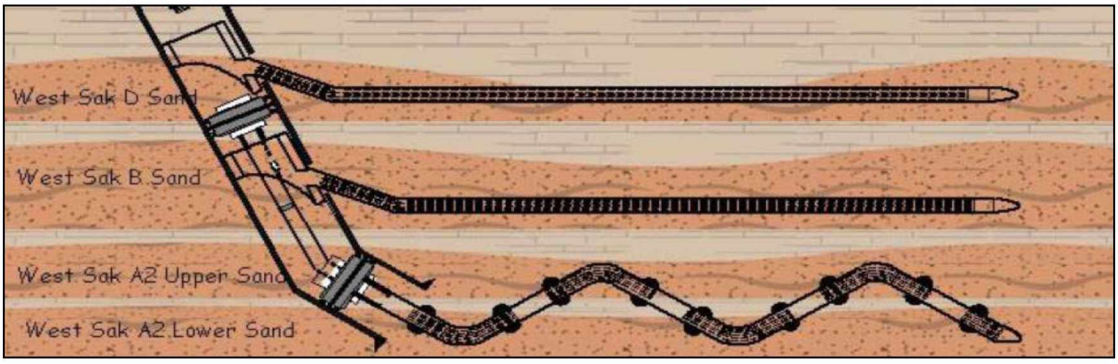

Figure 4: Optimum well design in West Sak reservoir (Targac et al., 2005)

2.3 Gas Injection Mechanisms

The idea of injecting miscible fluids in oil reservoirs in order to increase oil recovery dates back to the 1920s. However, major developments in understanding of the mechanisms started in the 1950s (Blackwell et al., 1960).

Whorton and Kieschnick (1950) conducted different coreflood experiments using lean and enriched gases. They reported that increasing injection pressure above the bubble point pressure increases oil recovery. They observed that injected gas becomes richer in heavy components and that oil becomes richer in light components upon multiple contacts between injected CO_2 and reservoir oil. They proposed that this phenomenon has significant effect on the displacement process.

Stone and Crump (1956) evaluated the effect of gas composition on oil recovery. They reported that oil recovery increases when the injected gas is enriched with the intermediate components. They suggested that condensation of intermediate components of the injected gas into the oil phase is the main reason for increased oil recovery. Later, these mechanisms were named the vaporizing-gas drive and the condensing-gas drive, respectively (Stalkup,1983).

Hutchinson and Braun (1961) reported that low oil recovery in immiscible displacements is due to interfacial tension between injected fluid and in-place oil. Miscible displacement eliminates the interfacial tension, and high oil recovery can be achieved. They utilized ternary diagrams to illustrate the mechanisms of vaporizing-gas and condensing-gas drive miscible displacements. They also used these diagrams to show the minimum pressure and minimum enrichment required to develop miscibility in the vaporizing- and condensing-gas drive displacements. These conditions were then called minimum miscibility pressure (MMP) and minimum miscibility enrichment (MME), respectively.

Later, Zick (1986) reported that in most cases the results of enriched gas injection cannot be explained completely by the condensing-gas drive mechanism. He introduced a new mechanism, the condensing/vaporizing mechanism, and showed its accuracy in

interpreting experimental and simulation results. He stated that although the displacement yields a high oil recovery and seems to be miscible, true miscibility does not develop. He also showed that ternary diagrams do not efficiently illustrate this mechanism.

2.4 Carbon Dioxide EOR

Application of CO_2 as an EOR agent started decades ago due to its lower cost compared to miscible chemical solvents. Beeson and Ortloff (1959) conducted different coreflood experiments using CO_2 as injection gas. They reported that injecting CO_2 enhances oil recovery beyond the waterflood oil recovery. They attributed this increased recovery to the oil swelling and viscosity reduction mechanisms.

Depending on reservoir pressure, temperature, and oil composition, CO_2–oil displacement can be miscible or immiscible. For a specific oil at reservoir conditions, when the pressure is above MMP, CO_2 develops miscibility with oil upon multiple contacts. The residual oil saturation is decreased due to considerable reduction in interfacial tension between oil and injectant. One of the advantages of CO_2 over lean gas is that it develops miscibility at lower pressure (i.e., MMP is lower for CO_2 injection). Miscibility pressure of CO_2 can be as low as 1200 psia, and it increases with increasing reservoir temperature and decreasing oil gravity (Stalkup, 1983).

Holm (1976) reported that the mechanism of CO_2 miscible displacement is similar to that of high-pressure gas (vaporizing-gas drive); however, CO_2 extracts the heavy components (C5–C30) and achieving miscibility does not depend on existence of light intermediate components (C3–C4) in the reservoir oil.

Metcalfe and Yarborough (1979) suggested that the CO_2-oil miscibility mechanism is a function of reservoir temperature. At high reservoir temperatures (>120°F), miscibility is achieved by a vaporizing-gas mechanism, but at low reservoir temperatures (<120°F) miscibility is achieved through a condensing-gas drive mechanism.

If the pressure is below MMP, miscibility does not develop, but CO_2 dissolves in the oil phase to some extent, depending on pressure, temperature, and oil composition. This dissolution decreases the oil viscosity and causes oil swelling. Consequently, oil recovery increases (Beeson and Ortloff, 1959; Simon and Graue, 1965).

Chung et al. (1988) conducted slim tube and coreflooding tests on a viscous oil using CO_2 as injection gas. The CO_2 - oil displacement was immiscible. They reported that CO_2 dissolution reduces oil viscosity by 84% and yields a swelling factor of 1.2. This increased oil recovery by 33% OOIP over waterflood.

Goodrich (1980) reported promising results from injecting CO_2 into two heavy oil reservoirs in Arkansas. He reported that oil swelling and viscosity reduction were the mechanisms responsible for increased oil recovery.

Khataniar et al. (1999) conducted slim tube and coreflood experiments using CO_2, Prudhoe Bay gas (PBG), and NGL enriched mixtures to displace Schrader Bluff viscous oil. They reported that CO_2 yielded better oil recovery than other mixtures. Injecting a single 0.05 PV CO_2 slug yielded the highest incremental oil recovery per injected gas volume.

Ning et al. (2011) evaluated the injection of CO_2 and enriched CO_2 into a sample ANS viscous oil reservoir. They reported that injecting 30% hydrocarbon pore volume (HCPV) CO_2 into the reservoir increased oil recovery by 10% OOIP. In this process, oil viscosity decreased by 85%, from 122 cp to 18 cp.

2.4.1 CO_2 Sequestration through EOR

In addition to increased oil recovery, CO_2 is also sequestered in the reservoir during CO_2 EOR. The sequestered CO_2 occupies the pore space previously filled with oil and is partially dissolved in residual oil and water (Orr, 2004).

In the EOR process, it is optimal to minimize the injected CO_2 per increased oil production in order to decrease EOR cost. If the objective of the project is sequestration and EOR, it is favorable to increase both the sequestered CO_2 volume and the oil recovery.

2.5 Water Alternating Gas (WAG)

Despite promising results of miscible/immiscible gas displacement in laboratory experiments, the first field application results were not successful (Rao, 2001). Due to low viscosity of the injected gas, high mobility ratio and heterogeneity of the reservoir, the process was impeded by viscous fingering and channeling. This caused early breakthrough, with the injected gas not contacting a large portion of the reservoir oil. This reduced the incremental oil recovery to only 5–10% OOIP (Rao, 2001).

Researchers suggested different methods to control mobility of the injected gases, including foam (Holm, 1970) and surfactant (Bernard et al., 1980) injection. However, these methods were never applied on a large scale. Caudle and Dyes (1958) suggested that injecting gas slugs alternating with water slugs, i.e. water-alternating-gas (WAG) injection, would solve this problem. Water slugs lower gas mobility and decrease viscous fingering and channeling. They reported that WAG increased the sweep efficiency over the continuous gas injection with the injected gas contacting more reservoir oil and consequently yielding a higher oil recovery. Blackwell et al. (1960) observed similar results in their experiments. They reported that effective mobility for WAG flooding was close to waterflooding mobility and significantly lower than gas flooding mobility. Wang and Locke (1980) conducted a coreflooding experiment, displacing an oil sample using water-alternating-CO_2 slugs. They changed the sequences of these slugs and reported no significant effect on oil recovery. However, the change did decrease the producing gas oil ratio (GOR).

Summaries of CO_2 injection field results are reported in Goodrich (1980) and in Brock and Bryan (1989).

2.6 Dissolution of CO_2 in the Aqueous Phase

Dissolution of CO_2 in aqueous phase can be significant when the water saturation is high (e.g., during WAG flooding). Enick and Klara (1992) conducted different 1D simulation case studies to evaluate the effect of CO_2 aqueous solubility on the simulation result. They observed small changes in oil recovery when CO_2 was injected continuously. However, when CO_2 was injected by WAG flooding, oil recovery decreased significantly. The effect was more significant when the CO_2 and water slug sizes decreased. Enick and Klara stated that density and viscosity of the water phase changed due to dissolution of CO_2. They expected that these changes could affect results significantly when 2D or 3D models are used.

Chang et al. (1998) developed a 3D simulator capable of capturing CO_2 solubility in water phase. They conducted different WAG simulation cases on a simple 3D model and reported that up to 10% of injected CO_2 could be dissolved or "lost" in the water phase. They reported that CO_2 dissolution in the water phase delays oil recovery and decreases final oil recovery.

Yan and Stenby (2009) conducted 1D simulation studies on different oil samples and injection scenarios. They found that capturing CO_2 solubility in the water phase significantly affects simulation results including oil recovery and breakthrough time. They reported that the difference between oil recovery values increases with increased initial water saturation, temperature, and decreased salinity. They also found that the difference between oil recovery values is maximized at pressures close to MMP.

Yan and Stenby (2010) reported that the significance of considering CO_2 dissolution in the water phase is case dependent. For any case study, they recommended conducting a quick 1D model simulation to evaluate this effect before evaluating it in full 3D scale.

2.7 Injection of CO_2 in West Sak Reservoir

McGuire et al. (2005) reported that estimated oil recovery from West Sak is about 21% OOIP, after 30 years of waterflooding. This leaves a considerable amount of oil for the tertiary production phase. Injection of CO_2 into the reservoir is one of the options to increase oil recovery. Due to the shallow depth of the reservoir and proximity to permafrost, the reservoir temperature in WSCA is about 75°F. The critical temperature of CO_2 is 87.9°F; therefore, at reservoir temperature of 75°F and initial reservoir pressure of 1600 psia, pure CO_2 will exhibit a partially supercritical liquid like phase (Figure 5). Formation of three hydrocarbon phases, two liquid and one vapor, and a solid phase, asphaltene, is reported when mixing CO_2 with oil even at temperatures above the critical temperature of CO_2 (Shelton and Yarborough, 1977; Orr et al., 1981; Henry and Metcalfe, 1983).

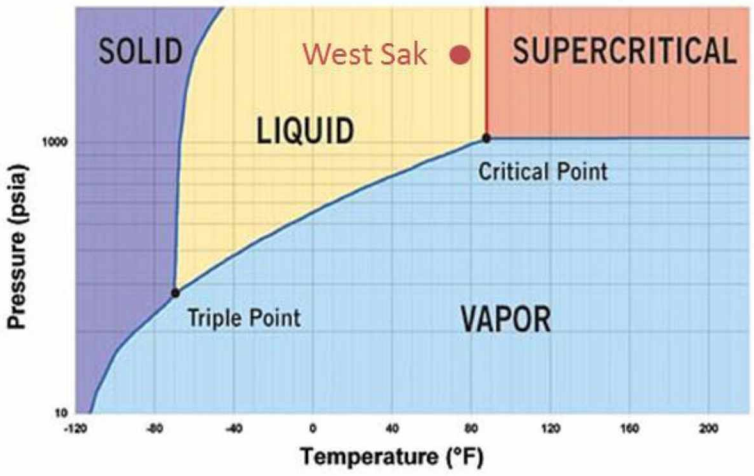

Figure 5: Phase diagram of CO_2 and West Sak reservoir pressure and temperature (red dot) (modified from Staub et al., 2004)

Shelton and Yarborough (1977) reported formation of multiple liquid equilibrium when mixing CO_2 with oil at low temperatures. They stated that precipitation of a solid phase is also possible when mixing CO_2 with asphaltic oil samples, which can reduce the relative permeability of the water phase and decrease the injectivity of the well.

Orr et al. (1981) reported that oil composition determines the maximum temperature at which multiple liquid equilibrium occurs. They proposed that 120°F is a good rule of thumb for this maximum temperature. They also reported that even in liquid-liquid equilibrium, CO_2 extracts the components from reservoir oil and develops miscibility.

Henry and Metcalfe (1983) conducted coreflooding experiments displacing three different oil samples with CO_2 inside a core-micromodel. They reported dynamic formation of liquid/liquid (L/L) and liquid/liquid/vapor (L/L/V) phase equilibriums in the core-micromodel.

Khan et al. (1992) developed a fluid characterization procedure to capture L/L and L/L/V equilibriums. They reported the efficiency of the procedure by tuning different equation of state (EOSs) for different West Texas oil samples. They also simulated different cases to evaluate the effect of capturing this complex phase behavior on the simulation results. They reported that considering L/L and L/L/V phase behavior might be important in evaluation of CO_2 injection into low temperature reservoirs.

Lim et al. (1992) evaluated CO_2 injection in the Monahans Clearfork reservoir. They conducted three- and four-phase simulation case studies. They reported that ignoring the second non-aqueous liquid phase overestimates the ultimate oil recovery by 4% original oil in place (OOIP), after 20 year of CO_2 and water injection. They did not report the total injected water and CO_2 volume for these simulation cases.

Wang and Strycker (2000) conducted a slim tube test and used CO_2 to displace a Schrader Bluff oil sample. They compared their experimental results with simulated results using the UTCOMP simulator and four-phase flow option. They reported that the UTCOMP could accurately simulate the process. They found that using the modified Corey relative permeability model (Dria et al. 1993) yielded the best match between simulated and experimental oil recovery values; the three-phase flow option could underestimate oil recovery by 5% OOIP.

Guler et al. (2001) reported that ignoring the second non-aqueous liquid phase, i.e., the CO_2-rich liquid, and including it in the gas phase could underestimate oil recovery and affect the saturation profile.

Lu (1994) conducted a three-phase flow compositional simulation study to evaluate CO_2 injection on a five-spot West Sak reservoir pattern model. He reported that waterflooding recovered about 30% OOIP, after injecting water for 20 years. Injecting one slug of 25% HCPV CO_2 increased oil recovery by about 22% OOIP, in addition to the waterflooding oil recovery. Injecting the same amount of CO_2 in two slugs increased the oil recovery 2% OOIP further, making the total oil recovery 54% OOIP.

Morye (2007) developed a fluid model for the West Sak reservoir and conducted three-phase simulation studies using different injection gases. He reported that injecting 10% HCPV of CO_2 recovered about 13% OOIP. Injecting 50% HCPV CO_2 could increase oil recovery up to 29% OOIP. He did not evaluate the oil recovery due to waterflooding.

2.8 Fluid Characterization

Accurate modeling of reservoir fluids is one of the most important factors in any compositional simulation study. In EOR gas injection projects, composition of the gas and oil changes continuously due to mass transfer between phases. Since it is impractical to experimentally evaluate the properties of reservoir fluids under all possible pressures and compositions, an equation of state (EOS) is used to simulate the properties of reservoir fluids

EOS models are able to simulate phase behavior of fluids with well-defined components. Accurate critical properties, acentric factors, and binary interaction coefficients are required for this purpose. Oil reservoir fluids, however, are complicated mixtures. They consist of light to very heavy components. It is impractical to determine the exact composition and properties of each component in such fluids.

In reservoir simulation studies, heavy components are lumped together and represented as several pseudo-components to better characterize the fluid. Due to uncertainties in the properties of these pseudo-components and interaction between different components, the property calculation of each phase using EOS bears some degree of uncertainty. Therefore, properties of the heavy pseudo-components and interaction parameters are regressed to tune the EOS by matching the laboratory results. A tuned EOS can accurately model the reservoir fluid behavior and improve the quality of the results in a compositional reservoir study.

A comprehensive procedure was proposed by Wang and Pope (2001) and Al-Meshari and McCain (2005) to tune the EOS for different oil samples. Their proposed procedure is as follows:

1. Build pseudo-components:
    a. Splitting is conducted to develop the extended composition that is required for accurate modeling of complex behavior of reservoir fluids in gas condensate or volatile oil reservoirs.
    b. Critical properties and acentric factors are calculated using different correlations.
    c. Lumping of components is done to reduce their total number, since the computational time of any compositional simulation study increases with increasing number of components.
    d. Critical properties and acentric factors of new groups are calculated using mixing rules.
2. Evaluate EOS and experimental results
3. Tune EOS:
    a. A reliable PVT data set is selected
    b. Regression parameters are selected
    c. With PVT software or manual techniques, the EOS is tuned

   i. Saturation pressure is matched using the molecular weight of plus fraction as tuning variable
   ii. Volumetric results are matched
   iii. Viscosity values are matched
4. Evaluate EOS performance in simulating other tests

Sharma (1990) reported that a mixture of 20 mol% West Sak oil and 80 mol% pure CO_2 forms three hydrocarbon (HC) phases in 1119.7 to 1214.7 psia pressure range: oil, CO_2-rich liquid, and CO_2-rich vapor. Therefore, the tuned EOS should be able to capture the phase boundaries.

Khan et al. (1992) suggested a comprehensive procedure to tune the EOS capable of modeling L/L/V equilibriums. They verified the efficiency of the procedure by tuning the EOS for different reservoir oils.

2.9 Simulator Description

When this study began, commercially available simulators were incapable of modeling the L/L/V equilibrium and four-phase flow simulation. A three dimensional compositional simulator, UTCOMP, developed in the Center for Petroleum and Geosystems Engineering at the University of Texas Austin, is used for this study. It is capable of handling four phases including water, oil, gas, and a second hydrocarbon (HC) liquid phase. Chang (1990) provided a comprehensive description of the simulator. Here is a brief introduction:

UTCOMP conducts the Gibbs free energy test to determine the number of phases. Flash calculations are then conducted to determine the composition of each phase. The Peng-Robinson (Peng and Robinson, 1976) and the modified version of the Redlich-Kwong (RKES) (Turek et al., 1984) are available EOS options. Viscosity of the water is assigned as constant in input file and remains constant through the simulation. The viscosity values of oil, gas, and the second HC liquid phase are calculated using the Lohrenz correlation

(Lohrenz et al., 1964). UTCOMP provides vertical and horizontal well options in which wells can be controlled by constant rate or constant bottom-hole pressure.

Chapter Three: Methodology and Model Construction

During simulation studies, 1D and 3D models complement each other. Simplified coreflooding experiments can be simulated by 1D models. For this study, the 1D results are helpful for understanding the mechanism in EOR/sequestration. The effect of different parameters can also be evaluated quickly. Since 1D models exclude the viscous fingering and gravity segregation effect, results are easier to interpret compared to 3D pattern models. On the other hand, 3D pattern models are helpful for understanding the effect of areal and vertical reservoir parameter variations on the results. These models are representative of the entire reservoir or part of it. Therefore, they can be used to estimate increased oil recovery due to CO_2 injection and sequestered CO_2 volume at field scale.

3.1 The 1D Model

Three different 1D models were built to represent the different rock types of West Sak sand: D, B, and A. The models represented core samples having the size of 150, 0.15, and 0.15 ft in the x, y, and z directions. Grid size in the x direction was 0.1 ft to minimize numerical dispersion, a numerical error in calculation of saturation and concentration movement that causes smeared flood front. Porosity and permeability values of the models were 0.34 and 300, respectively. Initial water saturation was set equal to the irreducible water saturation of the associated rock type. Relative permeability data of all three rock types are presented in Section 3.4.

3.2 The 3D Pattern Model

Porosity, permeability, and water saturation data of well WS1-01 was obtained from the well-file-image database of the Alaska Oil and Gas Conservation Commission (AOGCC). A Stratigraphic Modified Lorenz (SML) plot of West Sak was generated using the core data (Figure 6). The results were used to define flow units (i.e., sand packages D, B, and A) and flow barriers (interbedded shale layers). Thirteen flow and barrier units and their corresponding thickness and average porosity values were calculated (Table 1). The porosity-permeability and porosity-water saturation cross plots

were also generated (Figures 7 and 8). Exponential trend lines were fitted to the data and the fitting parameters were obtained.

Table 1: West Sak flow units			
Layer Number	Thickness (ft)	Average Porosity	Sand Package
1	13	0.31	D
2	35	0.23	D
3	18	0.33	B
4	24.8	0.27	B
5	25.2	0.28	A
6	34.5	0.26	A
7	7	0.31	A
8	12.6	0.28	A
9	7.9	0.31	A
10	4	0.23	A
11	10	0.30	A
12	12	0.23	A
13	9.1	0.30	A

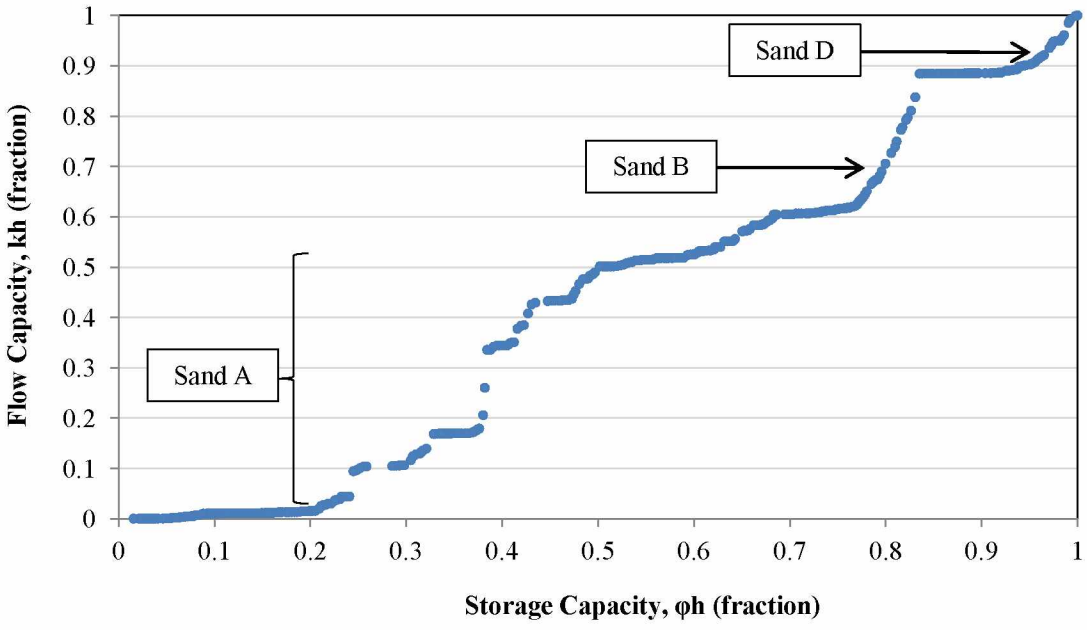

Figure 6: SML of West Sak Well WS 1-01

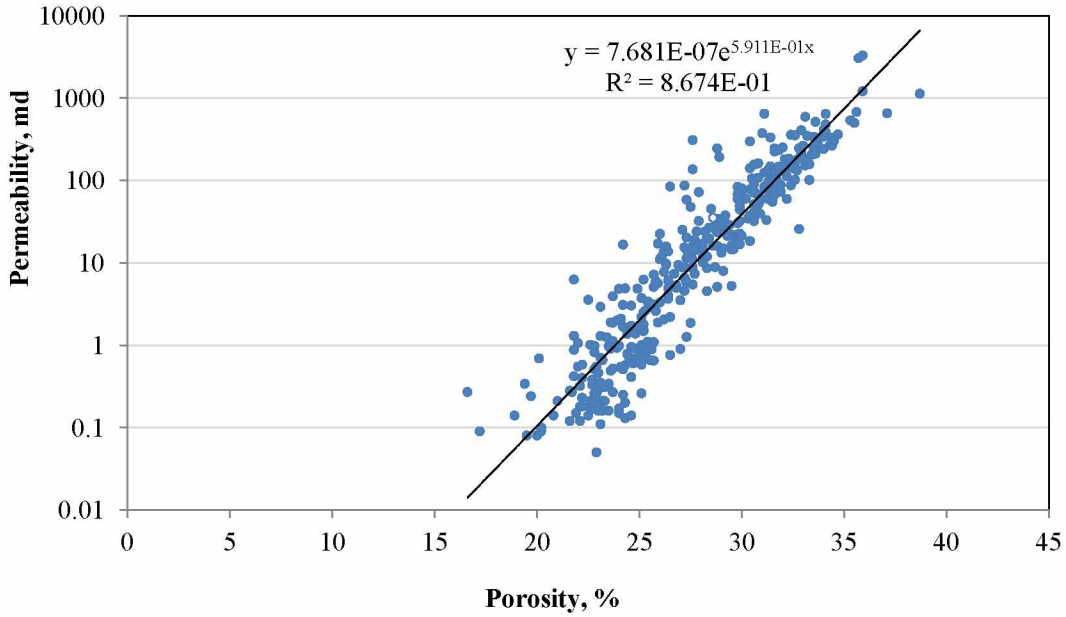

Figure 7: Porosity – permeability cross plot of Well WS1-01

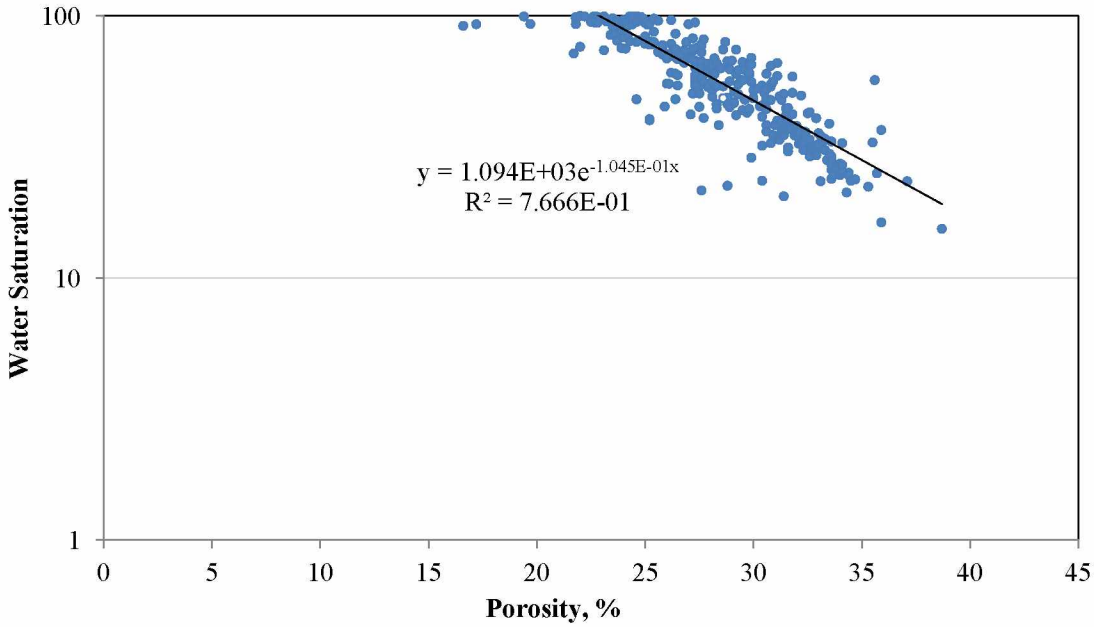

Figure 8: Porosity – water saturation cross plot of Well WS1-01

A homogenous model is not a good representation of the actual reservoir. It would also cause numerical anomalies in certain cases (NourpourAghbash and Ahmadi, 2012). The constructed heterogeneous model captures the variations in reservoir properties. The model is 1000, 1000, and 213.1 ft in the x, y, and z directions respectively. The grid sizes in x and y direction are 50 ft, small enough to prevent numerical dispersion and capture changes appropriately, while large enough to decrease total grid numbers and computational time. The porosity values of each layer were populated using the normal random distribution function. Calculated average porosity values were used as the mean values. The standard deviation of porosity was adjusted to 0.2 to yield permeability variation of over ±25%.

After building the 3D porosity model (Figure 9), the obtained exponential equations (see Figures 7 and 8) are used to calculate the permeability and water saturation values for each grid (Figures 10 and 11). The model does not necessarily capture all real reservoir heterogeneity; however, it is as representative as possible and prevents possible numerical anomalies.

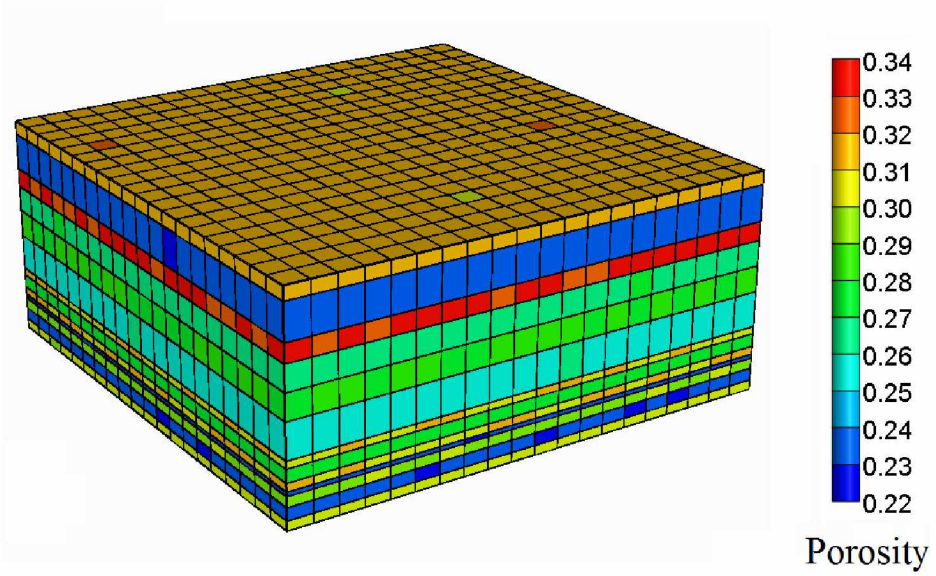

Figure 9: Porosity distribution of the pattern model

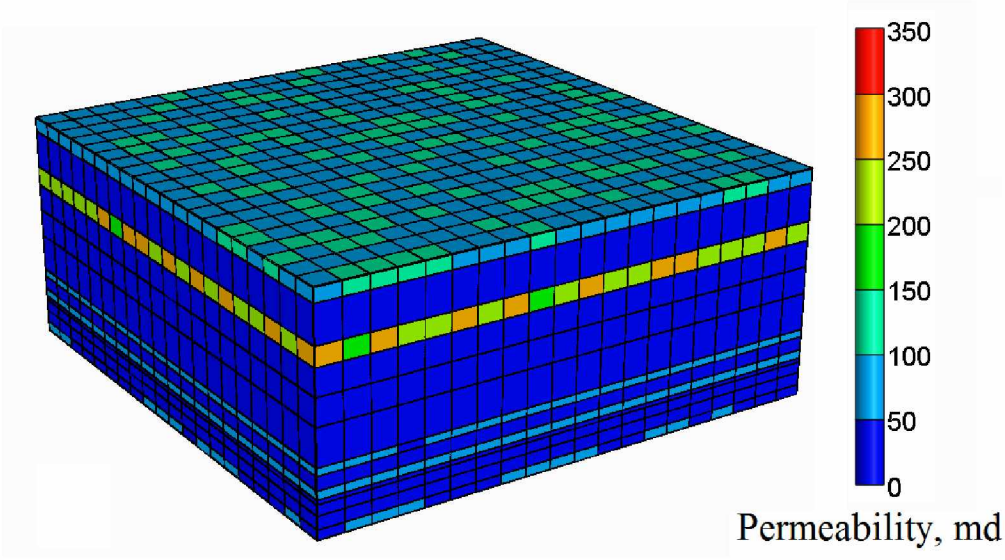

Figure 10: Permeability distribution of the pattern model

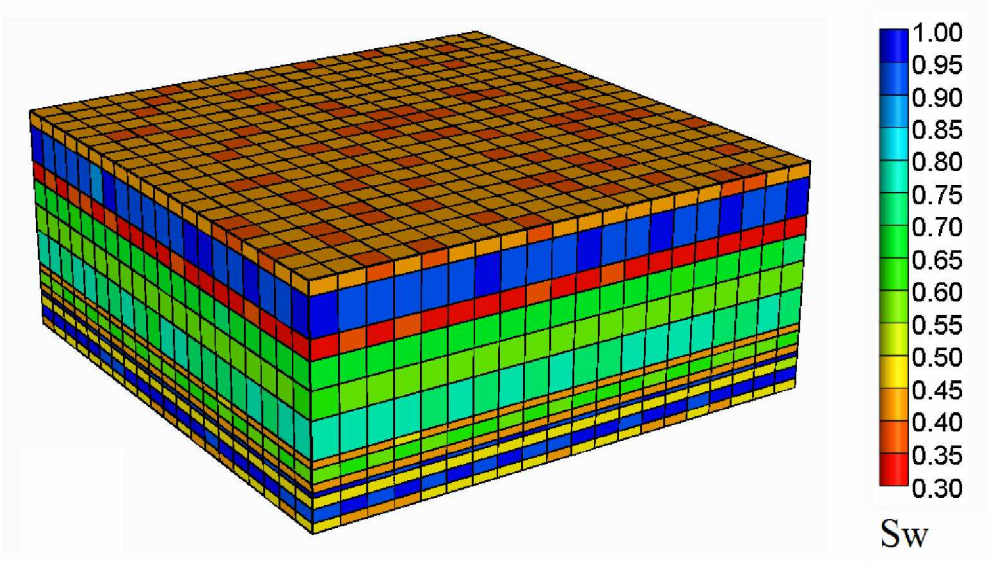

Figure 11: Water saturation distribution of the pattern model

3.3 Tuning of EOS

WinProp™, the PVT package of the CMG suite, was used to tune the EOS and build the reservoir fluid model. West Sak oil composition (Table 2) and PVT test results, including differential liberation (DL), constant composition expansion (CCE), and swelling test, were obtained from a previous study (Sharma, 1990). A combination of proposed procedures in Wang and Pope (2001), Al-Meshari and McCain (2005) and Khan et al. (1992) was used to develop the fluid model and tune the EOS.

The computational time of the compositional simulation studies increases with the increase in the number of components; therefore, using a minimum number of components is always recommended. Since West Sak oil contains a very low amount of N_2 (0.03 mol%), it was neglected in favor of decreasing the number of components and thus the computational time. The CO_2 and intermediate components were kept for use in evaluation of the injection of different mixtures. The Peng-Robinson EOS was selected. Using the gamma splitting function, the C_{21+} fraction was split up to C_{45+}.The Twu correlation (Twu, 1984) option was used for calculation of the critical properties. When the C_{7+} mole fraction is 0.4 to 0.6, Khan et al. (1992) recommended using three pseudo-components to model the L/L/V equilibriums accurately. Therefore, C_7–C_{45+} components were lumped into three pseudo-components (see Table 5).

The DL test was simulated, and results were compared to experimental values. The P_c, T_c, and acentric factor of pseudo-components were selected as regression parameters to match the experimental oil saturation pressure, oil density, gas oil ratio, gas specific gravity, and gas compressibility factor. In the regression process, higher weight was assigned to the saturation pressure due to the significance of accurate modeling of saturation pressure in correct phase identification. Table 3 shows selected EOS parameter values before and after regression for each pseudo-component.

Table 2: Composition of the West Sak oil	
Component	Mol%
CO2	0.02
N2	0.03
C1	38.25
C2	0.86
C3	0.36
NC4	0.18
NC5	0.06
C6	0.20
C7	0.02
C8	0.01
C9	0.82
C10	1.50
C11	1.72
C12	1.35
C13	1.50
C14	1.80
C15	1.94
C16	1.80
C17	1.57
C18	1.80
C19	2.46
C20	2.83
C21+ (MW=455,SG=0.875)	38.95

Table 3: Changes in values of EOS parameters									
Variable	Pc, Psia			Tc, R			Acentric Factor		
	Before	After	Change, %	Before	After	Change, %	Before	After	Change, %
C7-C17	295.97	333.87	12.81	1240.68	1199.18	-3.34	0.58	0.34	-41.15
C18-C30	175.13	216.31	23.51	1439.55	1307.18	-9.19	0.88	0.64	-27.17
C31+	104.89	128.13	22.15	1709.39	1451.18	-15.11	1.26	0.93	-26.85

Sharma (1990) conducted swelling tests on the West Sak oil with 60 mol% and 80 mol% of CO_2. He reported that when 80 mol% of CO_2 is mixed with 20 mol% West Sak oil, L/L/V equilibrium forms in the 1119.7 to 1214.7 psia pressure range. Binary interaction coefficients between CO_2 and other components were changed to match the experimental values for the swelling test and L/L/V phase boundaries.

Critical volume (V_c) of pseudo-components and Lohrenz correlation parameters were then selected as regression parameters to match the experimental values for oil and gas viscosities. Table 4 shows the V_c values before and after regression. Higher weight was given to oil viscosity due to its significance in simulation results. Considering the importance of the injected gas viscosity and density, very accurate simulated values for pure CO_2 were obtained from the National Institute of Standards and Technology (NIST) database. Simulated and NIST values were compared to check the accuracy of the tuned EOS. Figure 12 shows a summary of the tuning procedure for the EOS.

Table 4: Changes in Vc

Variable	Vc (viscosity), ft3/lb-mole		
	Before	After	Change, %
C7-C17	11.10057	25.347804	128.34694
C18-C30	19.06953	31.999188	67.802673
C31+	30.4404	38.866634	27.681108

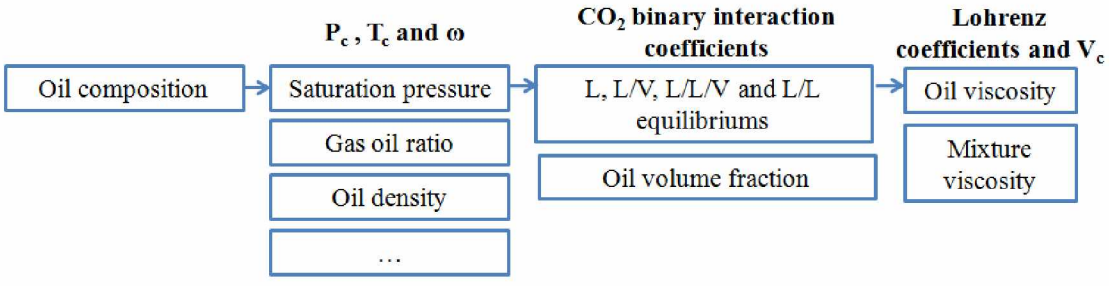

Figure 12: Tuning procedure for the EOS

Tables 5–7 show the tuned EOS parameters and coefficients of Lohrenz viscosity correlation. These parameters were used throughout this study.

The tuned EOS can accurately simulate the experimental value for all oil and gas properties. Figures 13–16 show the DL test results after the tuning. Predicted oil viscosity values at pressures below 500 psia deviate significantly from experimental values (Figure 15). Since the pressure range of the simulation model is 600–2500 psia, this poor match can be safely ignored. The simulated and experimental oil volume fractions for 80 mol% CO_2 and 20 mol% West Sak oil mixtures are shown in Figure 17. The results show that the EOS is capable of modeling the oil-swelling test.

A batch of three-phase flash calculation was conducted using UTCOMP, to generate pressure versus CO_2 concentration (P-X) plot of CO_2-oil mixtures. The tuned EOS captured the reported L/L/V boundaries accurately. Figure 18 shows the accuracy of the tuned EOS in capturing these boundaries and four different phase equilibriums for the CO_2-oil mixture. It also shows that CO_2-oil mixtures can form liquid (L) and liquid/vapor (L/V) equilibriums, in addition to previously discussed L/L and L/L/V equilibriums.

The experimental and NIST values of CO_2 density and viscosity are plotted in Figures 19 and 20. Sharma (1990) reported that mixing CO_2 with oil decreases oil viscosity by 75%. The EOS model successfully captured this viscosity reduction (Figure 21).

Comparison of experimental and simulated values verifies the accuracy and efficiency of the tuning procedure in this study.

Table 5: West Sak fluid description								
Component	Z, mole fraction	Pc, psia	Tc, R	Vc, ft^3/lb-mole	MW	Acentric Factor	Parachor	Volume Shift
CO2	0.000	1069.865	547.560	1.506	44.010	0.225	78.000	0.000
C1	0.382	667.196	343.080	1.586	16.043	0.008	77.000	0.000
C2	0.009	708.345	549.720	2.371	30.070	0.098	108.000	0.000
C3	0.004	615.760	665.640	3.252	44.097	0.152	150.300	0.000
NC4	0.002	551.098	765.360	4.085	58.124	0.193	189.900	0.000
NC5	0.001	489.375	845.280	4.870	72.151	0.251	231.500	0.000
FC6	0.002	477.030	913.500	5.510	86.000	0.275	250.100	0.000
C7-C17	0.140	333.875	1199.185	25.348	181.699	0.339	499.971	0.000
C18-C30	0.291	216.307	1307.185	31.999	326.686	0.639	803.632	0.000
C31+	0.170	128.131	1451.185	38.867	595.260	0.925	1088.620	0.000

Table 6: Binary interaction coefficients										
	CO2	C1	C2	C3	NC4	NC5	FC6	C7-C17	C18-C30	C31+
CO2	0.0000									
C1	0.0500	0.0000								
C2	0.0700	0.0027	0.0000							
C3	0.0700	0.0085	0.0017	0.0000						
NC4	0.0700	0.0147	0.0049	0.0009	0.0000					
NC5	0.0700	0.0206	0.0086	0.0027	0.0005	0.0000				
FC6	0.0700	0.0253	0.0117	0.0046	0.0015	0.0003	0.0000			
C7-C17	0.1100	0.0598	0.0382	0.0244	0.0163	0.0111	0.0080	0.0000		
C18-C30	0.1100	0.0952	0.0684	0.0500	0.0382	0.0302	0.0251	0.0049	0.0000	
C31+	0.150	0.1303	0.0998	0.0780	0.0636	0.0534	0.0467	0.0168	0.0036	0.0000

Table 7: Coefficients of Lohrenz viscosity correlation				
Coefficient 1	Coefficient 2	Coefficient 3	Coefficient 4	Coefficient 5
0.1006	0.0127	0.0588	-0.0277	0.0047

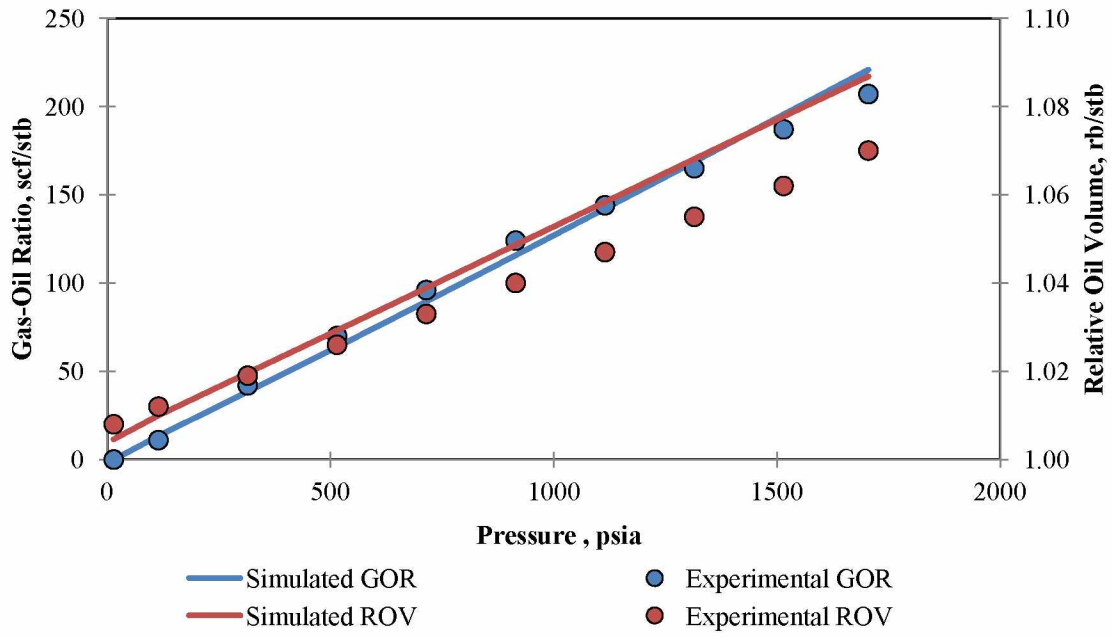

Figure 13: Simulated and experimental gas oil ratio (GOR) and relative oil volume (ROV)

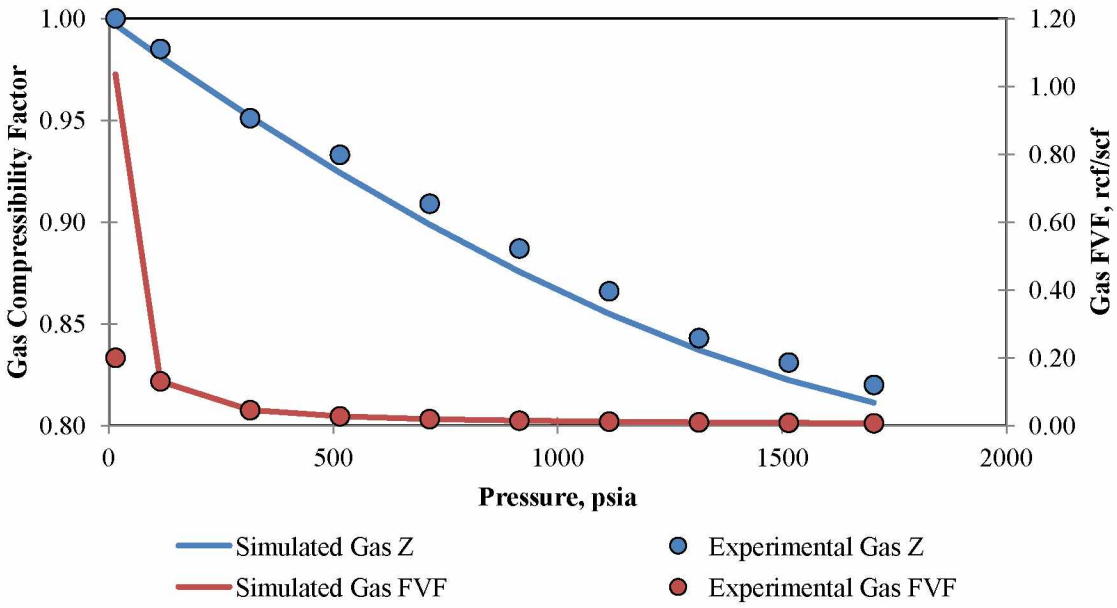

Figure 14: Simulated and experimental gas compressibility factor (z) and gas formation volume factor (FVF)

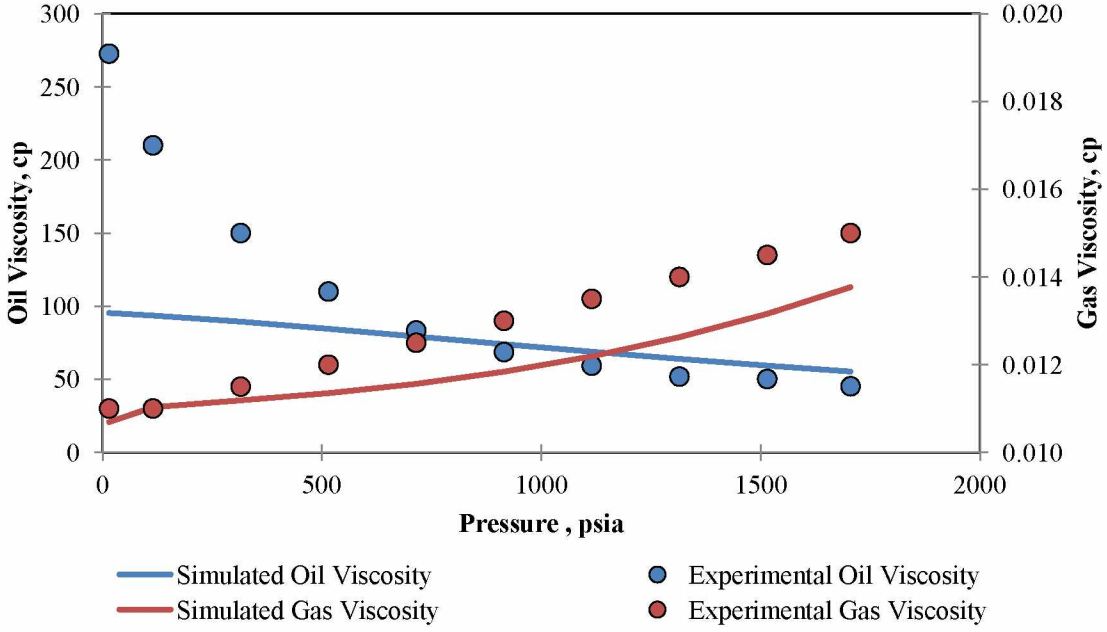

Figure 15: Simulated and experimental oil and gas viscosity

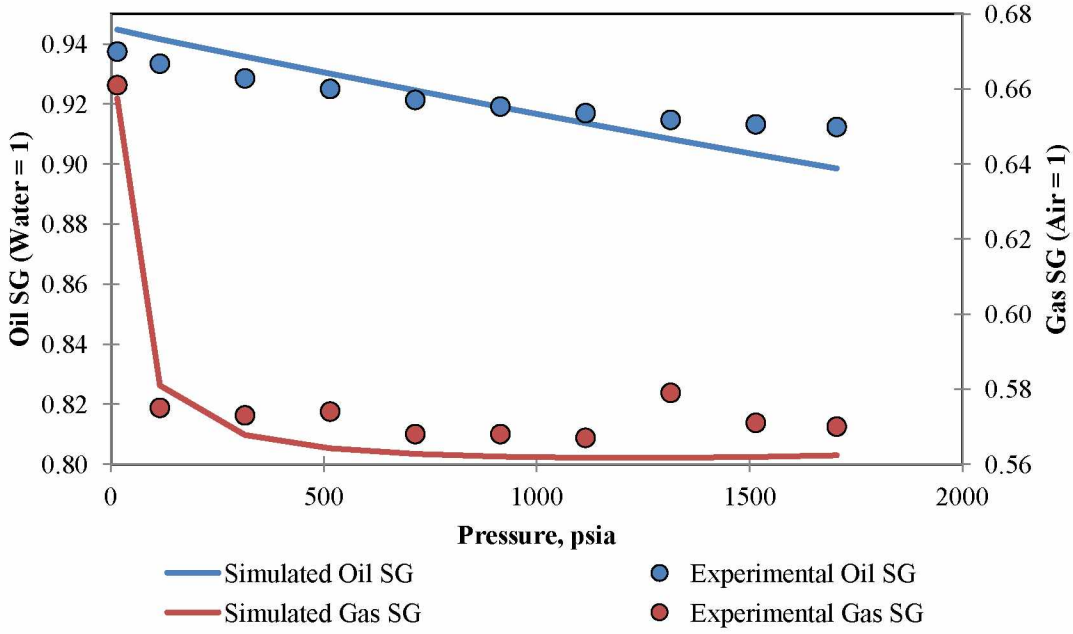

Figure 16: Simulated and experimental oil and gas specific gravity (SG)

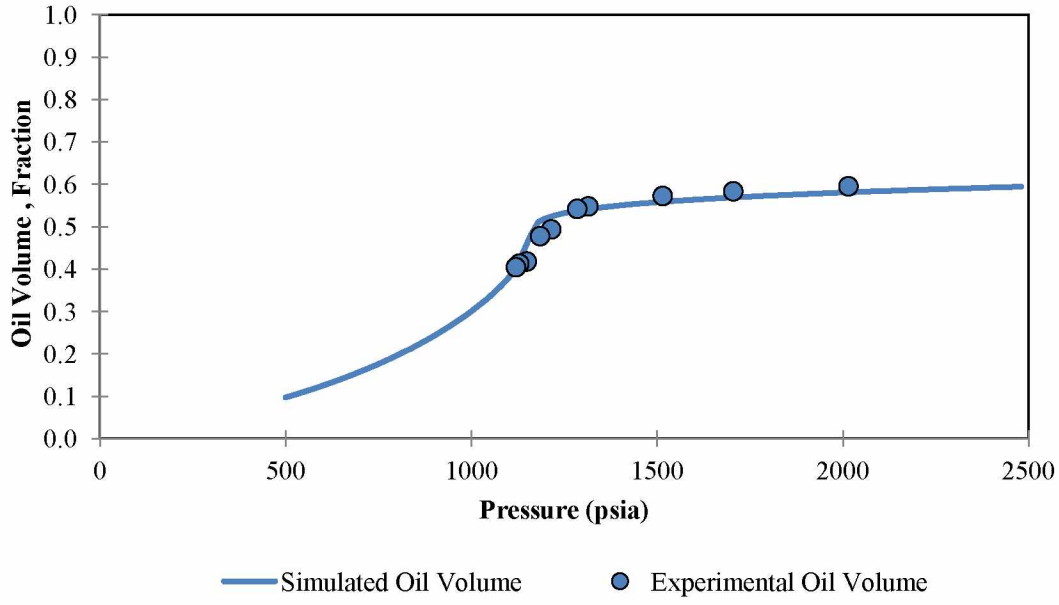

Figure 17: Oil volume fraction for 80 mol% CO_2 and 20 mol% West Sak oil mixture

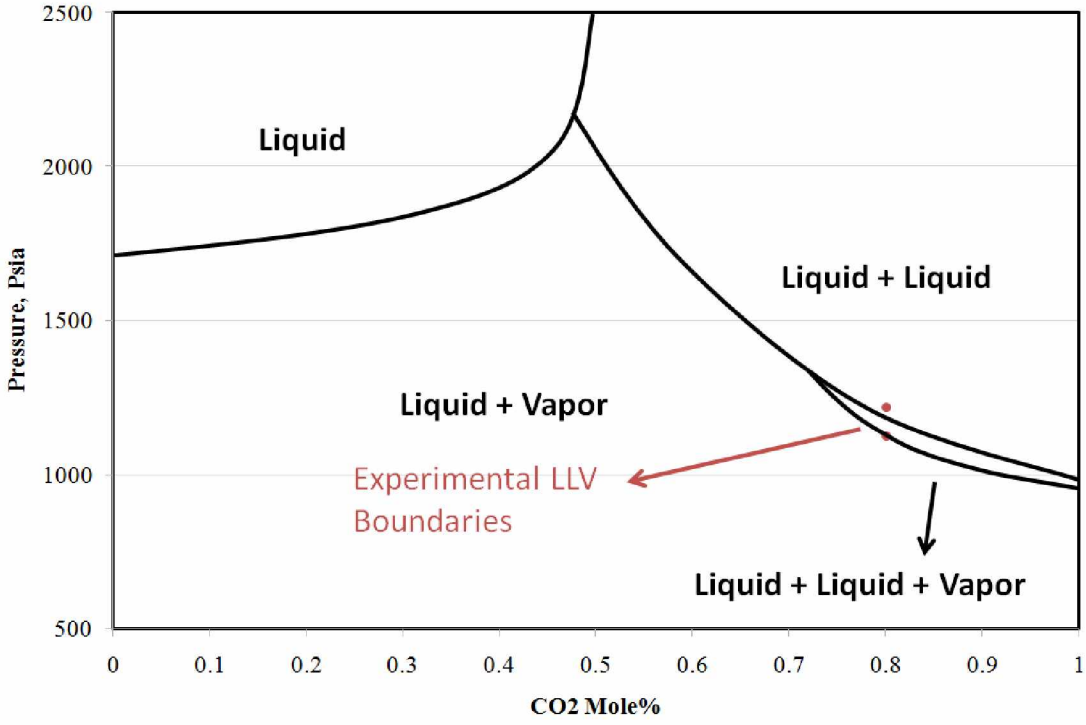

Figure 18: Simulated (solid black lines) and experimental (pink dots) phase equilibriums

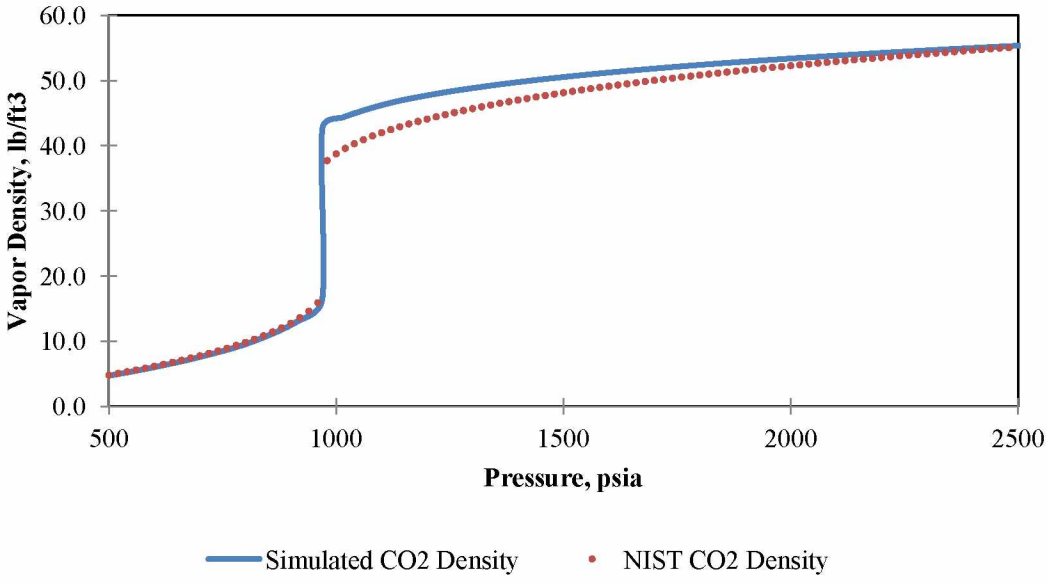

Figure 19: Simulated and NIST density of pure CO_2

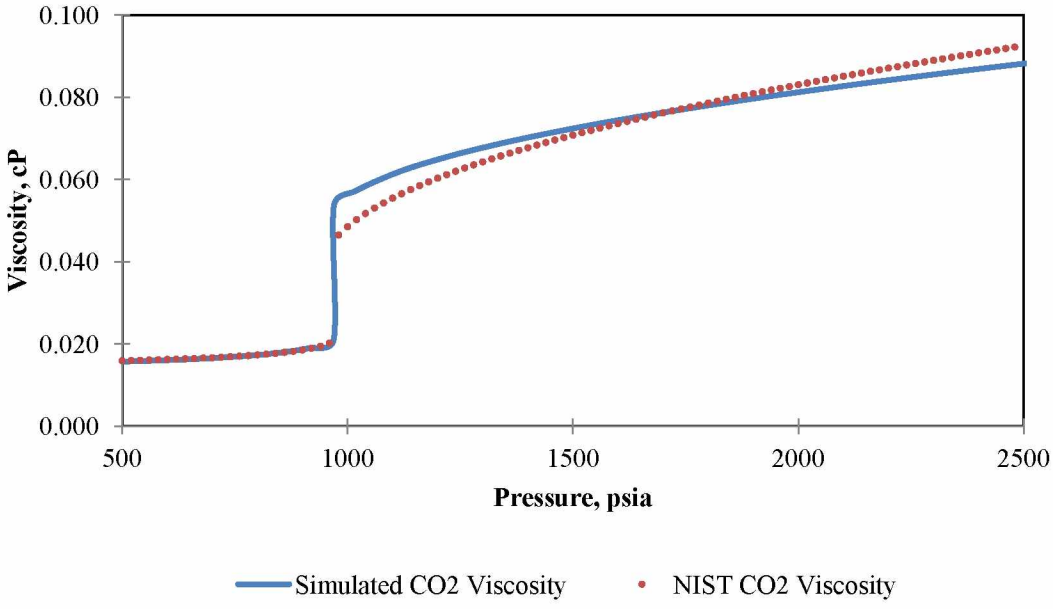

Figure 20: Simulated and NIST viscosity of pure CO_2

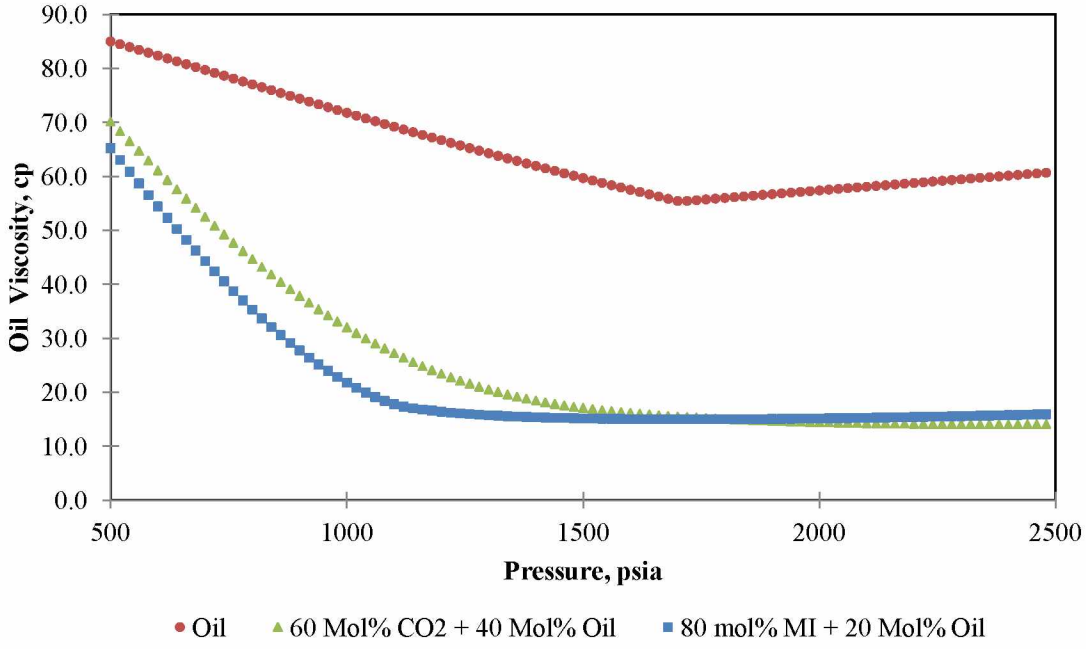

Figure 21: Simulated viscosity of oil and CO_2-oil mixtures

3.4 Relative Permeability

The relative permeability parameters for water, oil, and gas were obtained from a previous study (Bakshi, 1991). Since UTCOMP requires parametrical relative permeability input, Bakshi's graphical inputs were matched with parametrical inputs to obtain the UTCOMP relative permeability inputs. Benson (2006) conducted a drainage test with liquid CO_2 and water in a sandstone (K=300md). Due to similar characteristics of this sandstone and West Sak sand packages, Benson's test results were matched with parametrical inputs to obtain relative permeability parameters of the second HC liquid phase. Table 8 includes all relative permeability parameters used in this study.

Similar to West Sak oil, mixing Schrader Bluff oil and CO_2 forms three HC phases in certain pressures and CO_2 concentrations. Wang and Strycker (2000) conducted a slim tube test by flooding the Schrader Bluff oil with pure CO_2. They used different relative permeability models and compared the simulation results. They reported that the modified Corey model (Dria et al. 1993) gives the best match between experimental and

simulated oil recovery. Therefore, the modified Corey model was chosen in this study. Capillary pressure and the effect of interfacial tension on relative permeability were neglected in this study.

Table 8: Relative permeability specification			
Parameters of the Relative Permeability Model	Sand D	Sand B	Sand A
Residual Water Saturation (Swr)	0.35	0.33	0.44
Residual Oil Saturation for Water-Oil Flow(Sorw)	0.4	0.37	0.24
Residual Oil Saturation for Gas-Oil Flow(Sorg)	0.4	0.33	0.28
Residual Gas Saturation (Sgr)	0.1	0.1	0.1
Residual 2nd HC liquid Saturation for Water-2nd HC Liquid Flow (S4rw)	0.15	0.15	0.15
Residual 2nd HC liquid Saturation for Gas-2nd HC Liquid Flow (S4rg)	0.15	0.15	0.15
Water End-point Relative Permeability (K0rw)	0.145	0.057	0.19
Oil End-point Relative Permeability (K0ro)	1	1	1
Gas End-point Relative Permeability (K0rg)	1	1	1
2nd HC liquid End-point Relative Permeability (K0r4)	0.4	0.4	0.4
Water Relative Permeability Exponent (ew)	1.3	2	1.8
Oil Relative Permeability Exponent for Water-Oil Flow (eow)	2	2.5	2
Oil Relative Permeability Exponent for Gas-Oil Flow (eog)	3	3	2.5
Gas Relative Permeability Exponent (eg)	1.3	1	1.5
2nd HC Liquid Relative Permeability Exponent for Water-2nd HC Liquid Flow (e4w)	3	3	3
2nd HC Liquid Relative Permeability Exponent for Gas-2nd HC Liquid Flow (e4g)	3	3	3

3.5 Production/Injection Options

In 1D models, the initial pressure was 1710 psia, just above the West Sak oil bubble point pressure of 1704 psia. Water and CO_2 were injected with constant bottom-hole pressure of 1720 psia, and oil was produced at constant bottom-hole pressure of 1710 psia. Total water/CO_2 injection was 1.0 HCPV for waterflooding/CO_2 injection cases.

One trilateral injection and one trilateral production well were specified for 3D pattern model case studies. The laterals in sands D and B were horizontal, but the laterals in sand A2 were undulating (Figure 22).

Fracture parting pressure was calculated by multiplying the depth, 3500 ft, by the assumed fracture-parting gradient, 0.75 psi/ft. The injector was specified to operate with constant bottom-hole pressure of 2500 psia, slightly below fracture parting pressure. Targac et al. (2005) reported that in West Sak the production wells operate with 1000 psi

pressure drawdown. Therefore, in this study, the production well was set to operate in constant bottom-hole pressure of 600 psia.

In the waterflooding case, 1.0 HCPV of water was injected. In the base WAG case, 0.06 HPCV of CO_2 was injected with WAG ratio of 1 and slug sizes of 0.02 HCPV. Then, water was injected for a total CO_2-water injection of 1.0 HCPV.

Figure 23 shows the simulation procedure. The reservoir model was built using the prepared geological model, tuned EOS, relative permeability data, production/injection plan, etc. UTCOMP simulator was then used to generate the results.

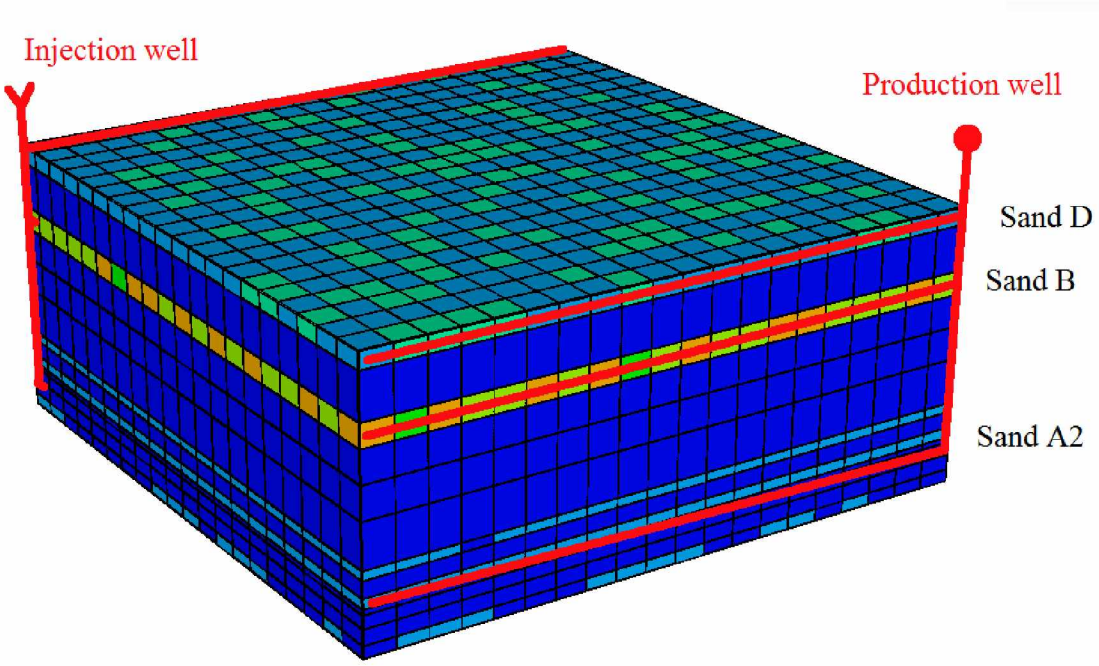

Figure 22: Well configuration in the 3D pattern model

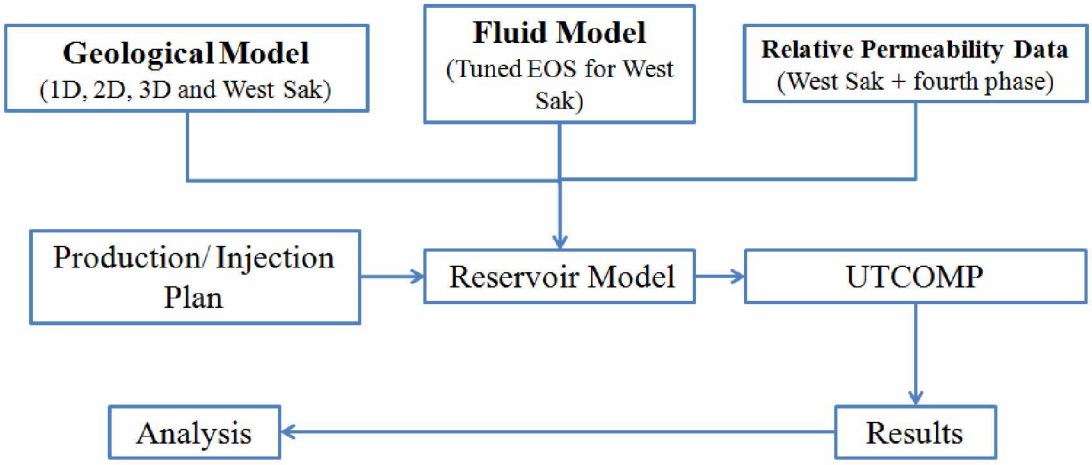

Figure 23: Simulation procedure diagram

Chapter Four: Results and Discussion

4.1 Waterflooding

Currently, waterflooding is the primary oil production mechanism in major parts of the West Sak reservoir. Due to interfacial tension between oil and water, viscosity contrasts, low sweep efficiency, etc., some oil will be left in the reservoir after waterflooding. This residual oil is the primary target of CO_2 injection. Oil recovery due to waterflooding operations is evaluated by the simulation cases. Then the efficiency of CO_2 injection can be determined by evaluation of incremental oil recovery over waterflooding.

4.1.1 The 1D Models

Figure 24 shows oil recovery for different rock types of West Sak reservoir after injection of 1.0 HCPV of water. Final oil recovery values for sand A and B cases are quite similar, 0.36 and 0.39 OOIP, and higher than the oil recovery value for sand D, 0.27 OOIP. The changes in the slope of oil recovery values correspond to the water breakthrough. The results show that water breakthrough occurs at different injected water volumes for each rock type.

Since all other parameters were kept the same, the difference in final oil recovery and water breakthrough values is due to different relative permeability parameters, such as irreducible water saturation, residual oil saturation and end-point relative permeability values. The results indicate that under ideal conditions of low water saturation and 100% sweep efficiency, waterflooding would be able to recover these amounts in each rock type.

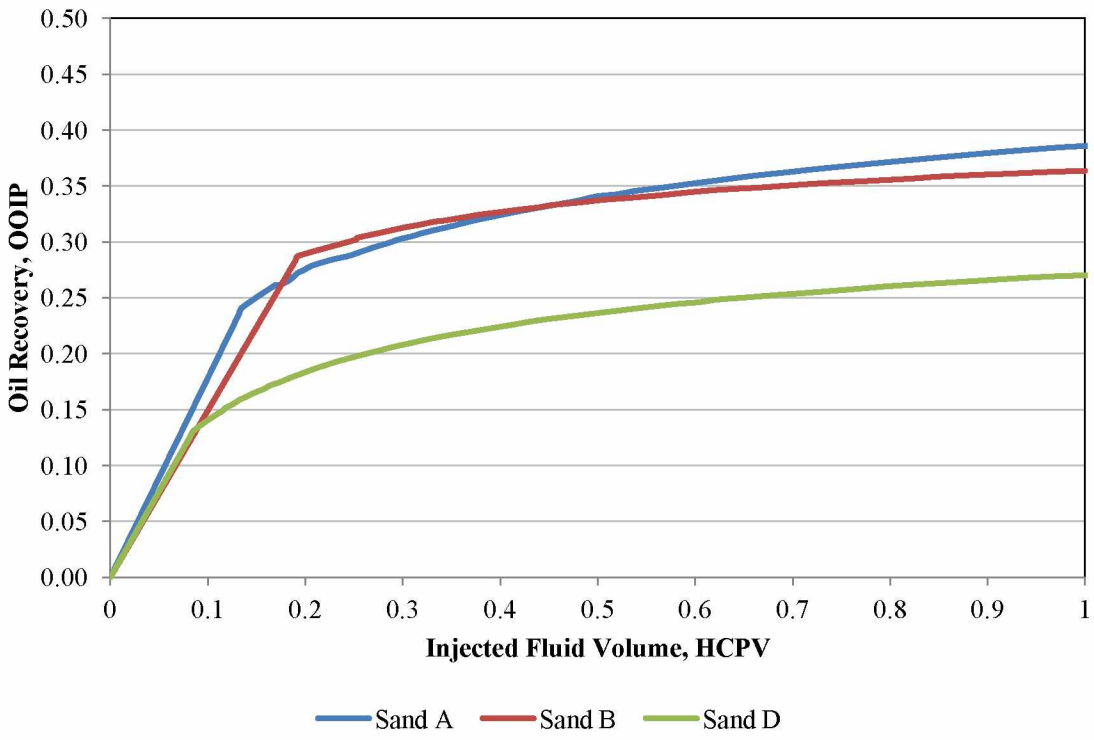

Figure 24: Waterflood oil recovery in different West Sak rock types

4.1.2 The 3D Pattern Model

In the 3D pattern simulation, oil recovery with waterflooding reached 0.14 OOIP after injection of 1 HCPV (Figure 25).

McGuire et al. (2005) reported that oil recovery due to waterflood is about 0.21 OOIP in West Sak reservoir, after 30 years of water injection. They did not report the total injected water volume. The difference between the waterflooding oil recovery in McGuire's study and Figure 25 is probably due to difference in total injected water volume.

The oil recovery value is also lower than the values in 1D models. The results of waterflooding in 1D models showed that in ideal conditions of low water saturation and equal injected volume to all layers, the oil recovery would be about 0.27–0.39 OOIP depending on the abundance of each rock type in the reservoir. The 3D pattern model is

not as simple as the 1D models. Sand layer A2 is perforated, but sand layers A1, A3, and A4 are not perforated. Water is not injected into these layers and oil is not produced. Layers of sands D and B are much thicker and more permeable than those of sand A2; therefore, the water is not injected equally in the layers. Because of these differences between the 3D pattern model and 1D models, oil recovery after waterflooding is as low as 0.14 OOIP in 3D pattern model.

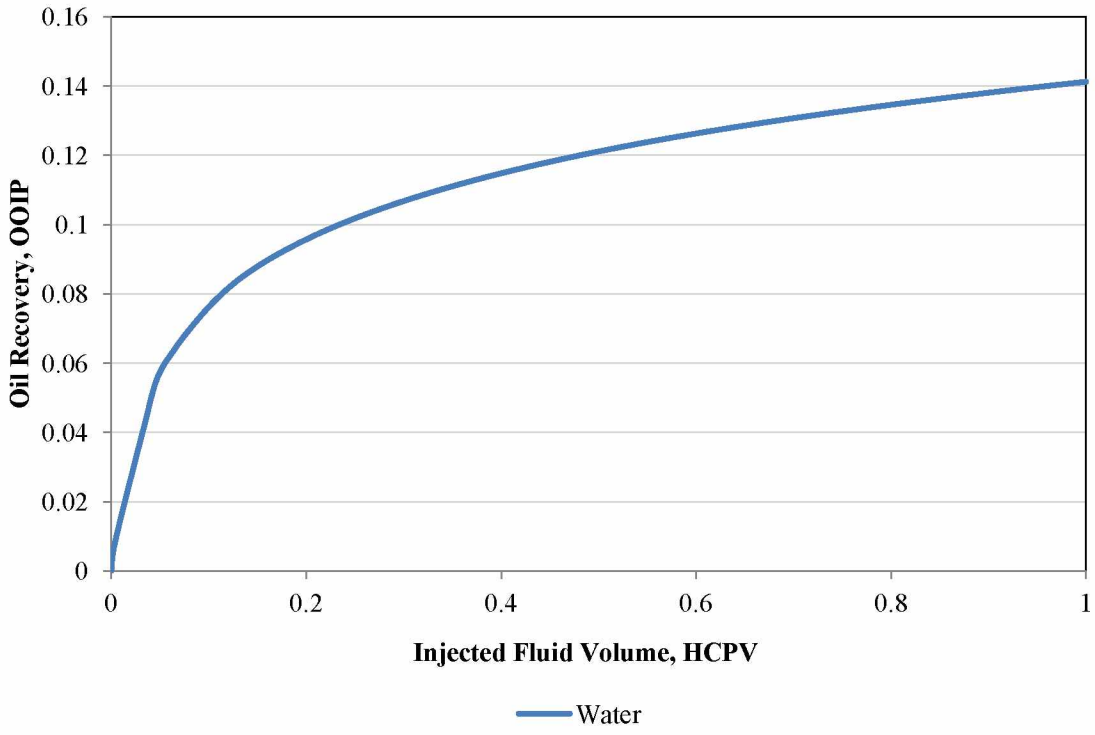

Figure 25: Oil recovery from waterflooding in 3D pattern model

4.2 CO_2 Injection

4.2.1 The 1D Model

Simplified CO_2 injection can be simulated by 1D models. Due to model simplicity, interaction between CO_2 and oil can be observed. This allows us to evaluate the effect of CO_2 on oil density and viscosity.

An injection of 0.25 HCPV water into the 1D models is followed by 0.25 HCPV CO_2. Water is then injected to reach total injected fluid volume of 1.0 HCPV. Figure 26 shows oil recovery for each rock type after this 1.0 HCPV CO_2 and water injection. The final oil recovery values had similar trend with oil recovery due to waterflooding. Changes in slope of oil recovery values correspond to water and CO_2 breakthroughs. The first change in oil recovery slope is due to water breakthrough and the second change is due to CO_2 breakthrough.

Oil recovery from sand A and B was nearly equal, 0.53 and 0.51 OOIP, and higher than oil recovery of sand D, 0.43 OOIP (Figure 27). These results indicate that CO_2 injection could increase oil recovery by 15% OOIP if the 0.25 HCPV volume of CO_2 is injected into all layers. However, since the layers have different properties, this probably will not happen.

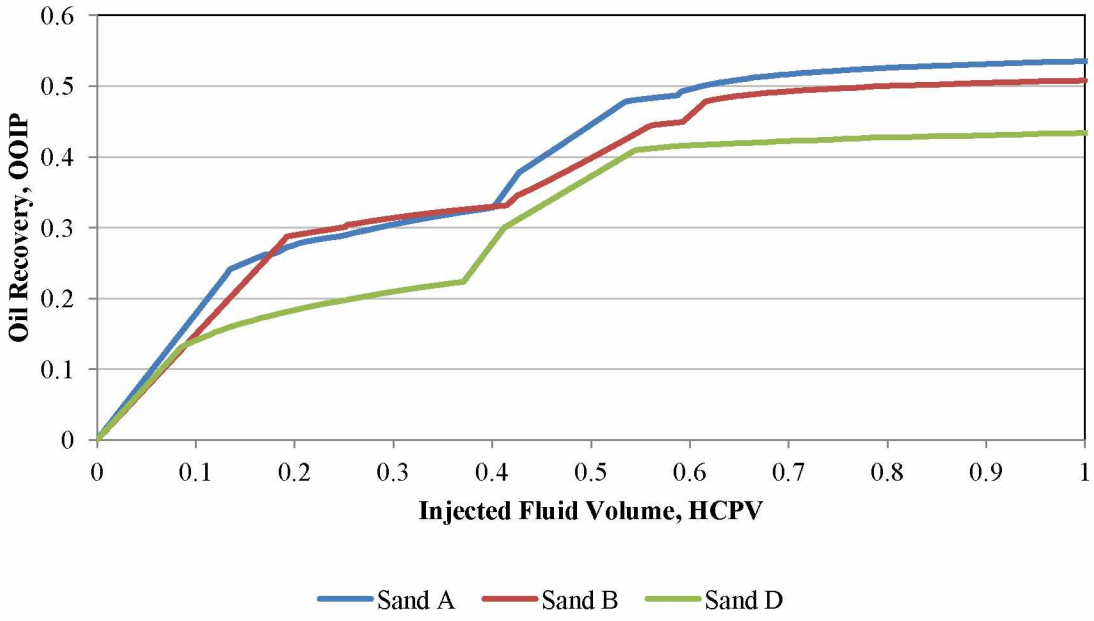

Figure 26: Oil recovery due to CO_2 WAG injection

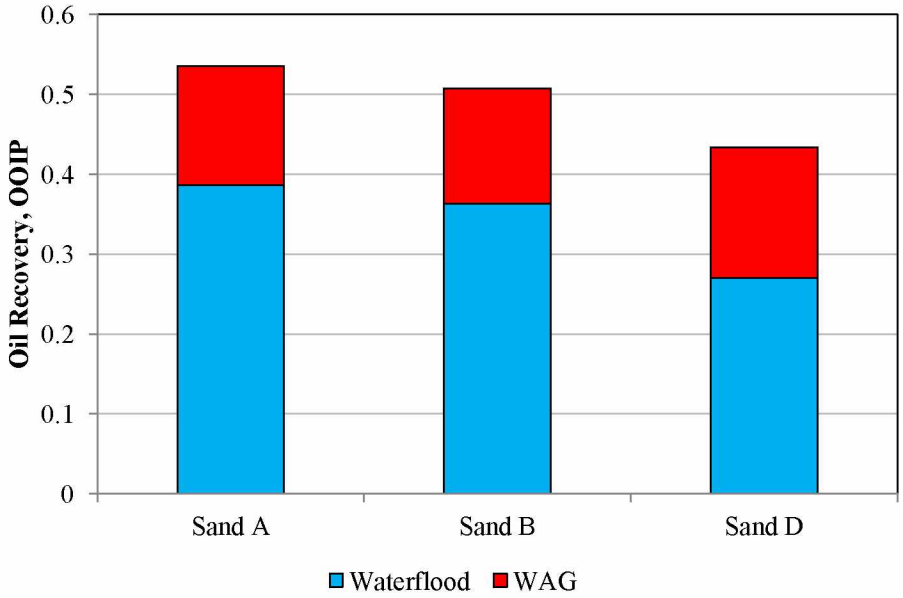

Figure 27: Oil recovery due to waterflooding and CO_2 WAG injection in different West Sak rock types

The mechanism of CO_2 injection was investigated in the 1D model of sand B. Since the fluid model is the same for all rock types, this mechanism is valid for the entire reservoir.

Figure 28 shows the model's saturation profile after injecting 0.4 HCPV water and CO_2 from the left side of the model. The x-axis shows the distance from the inlet and y-axis shows saturation values for different phases. The figure shows that injected CO_2 displaces the residual oil, recovering some of it and replacing it with second HC liquid phase. A gas bank moves ahead of the second HC liquid phase bank.

Figures 29–31 show the composition of oil, second HC liquid and gas phases after injecting 0.4 HCPV water and CO_2 from left side of the model. Similar to Figure 28, x-axes are distance from the inlet. The y-axes show the concentration of components and pseudo-components in each phase.

As CO_2 displaces the oil, two simultaneous mechanisms occur in the displacing front. The CO_2 dissolves in the oil, which causes the concentration of CO_2 in the oil phase to increase (Figure 29). At the same time, some C_1 and heavier components (intermediates) are vaporized into the CO_2-rich second HC liquid phase (Figure 30). Some C_1 also vaporizes and makes a separate gas phase ahead of this CO_2-rich bank (Figure 31). This gaseous phase moves faster than the CO_2 bank, due to lower viscosity and higher relative permeability of the gas phase. Figure 32 shows the effect of this phenomenon on effluent content. The C_1 content of produced oil and gas increases significantly around 0.42 HCPV showing the breakthrough of the front C_1-rich gas bank. The C_1 content of effluent oil and gas remains high until the entire gas bank is produced. CO_2-rich bank then breaks through, and CO_2 content peaks.

A similar mechanism was reported in Okuno et al. (2011) while displacing several west Texas oil with CO_2. Figure 33 shows the overall composition and the boundary of different phase equilibriums in their model. It shows that CO_2 mixes with oil and forms $L_1/L_2/V$ equilibrium. A portion of C_1 also vaporizes from the oil and accumulates in the front L_1-V region.

As CO_2 mixes with oil, density of the oil increases slightly (Figure 34). This increase is a combined effect of dissolved CO_2, striped C_1, and intermediates components which were discussed previously (see Figure 29). The effect of striped C_1 and intermediate components seems to suppress the effect of other mechanisms and cause oil density to increase.

Viscosity of the oil phase significantly decreases as CO_2 mixes with the oil phase (Figure 35). This viscosity reduction is one of the main mechanisms responsible for increased oil recovery after CO_2 injection. Figure 36 shows the viscosity of second HC liquid and gas phases.

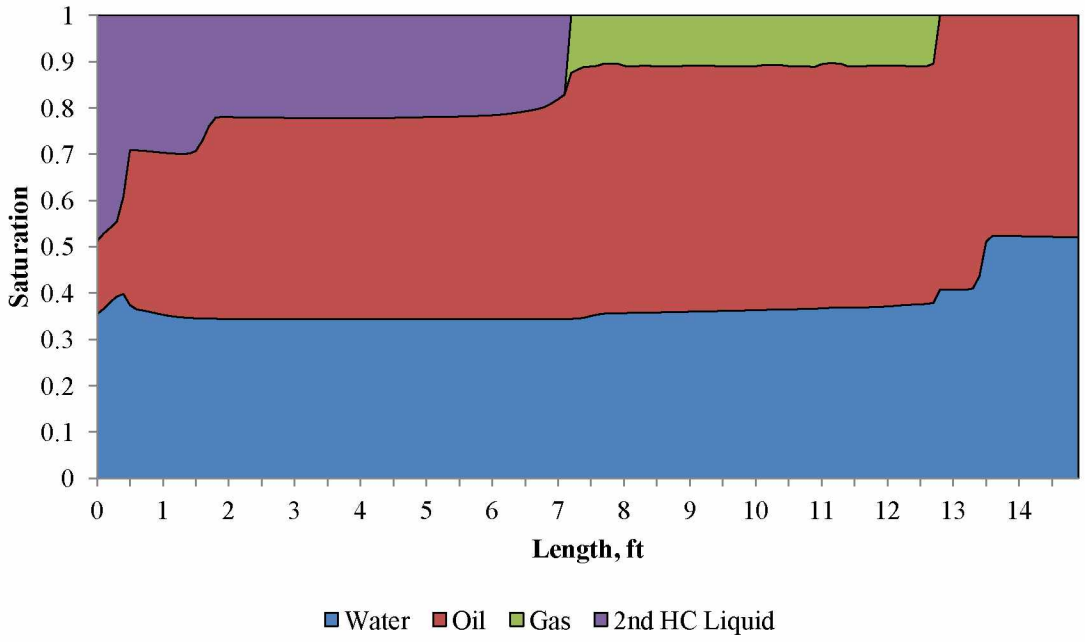

Figure 28: Saturation profile of sand B 1D model after injecting 0.4 HCPV water and CO_2

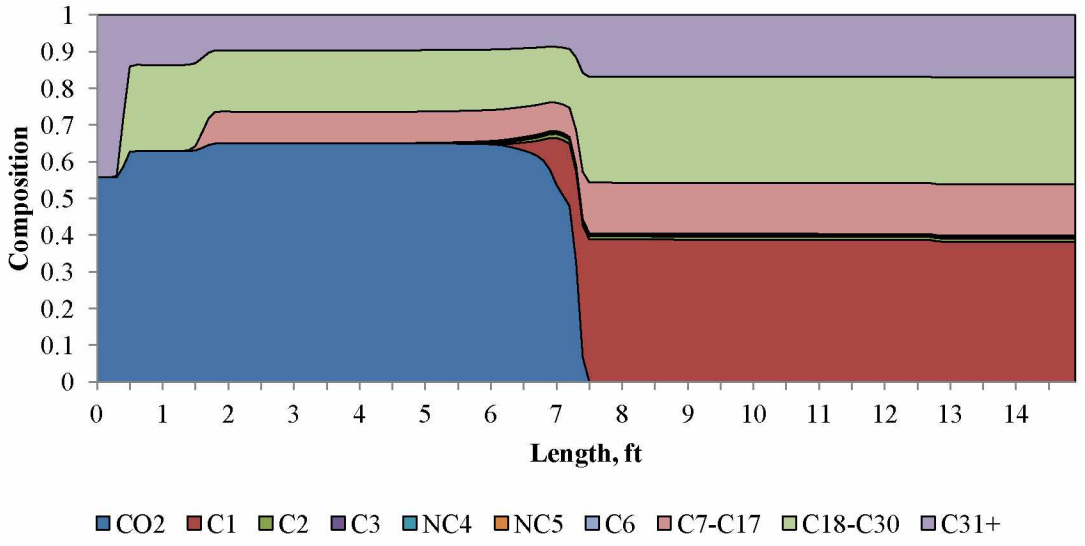

Figure 29: Composition of oil phase after injecting 0.4 HCPV water and CO_2

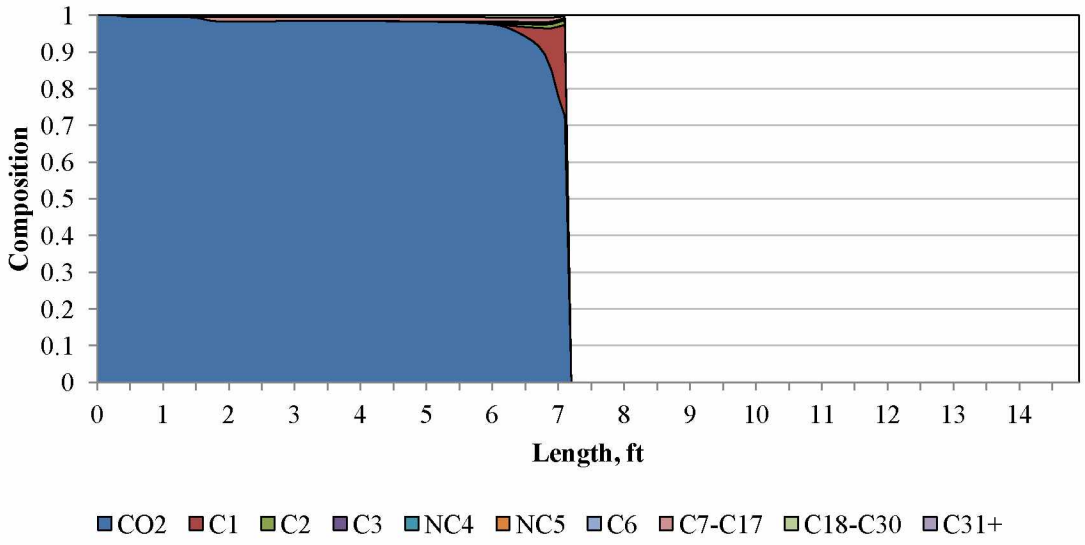

Figure 30: Composition of second HC liquid phase after injecting 0.4 HCPV water and CO_2

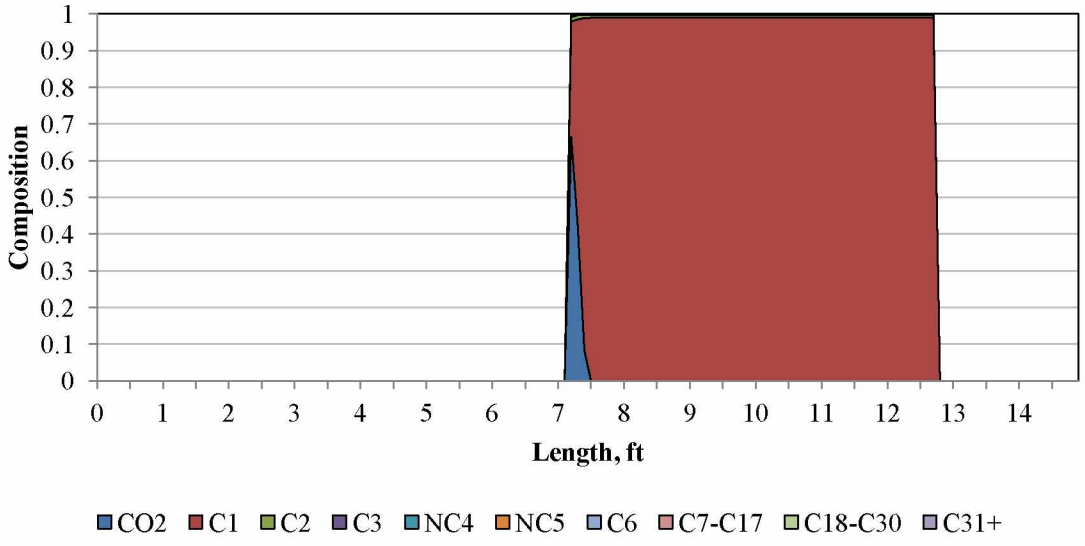

Figure 31: Composition of gas phase after injecting 0.4 HCPV water and CO_2

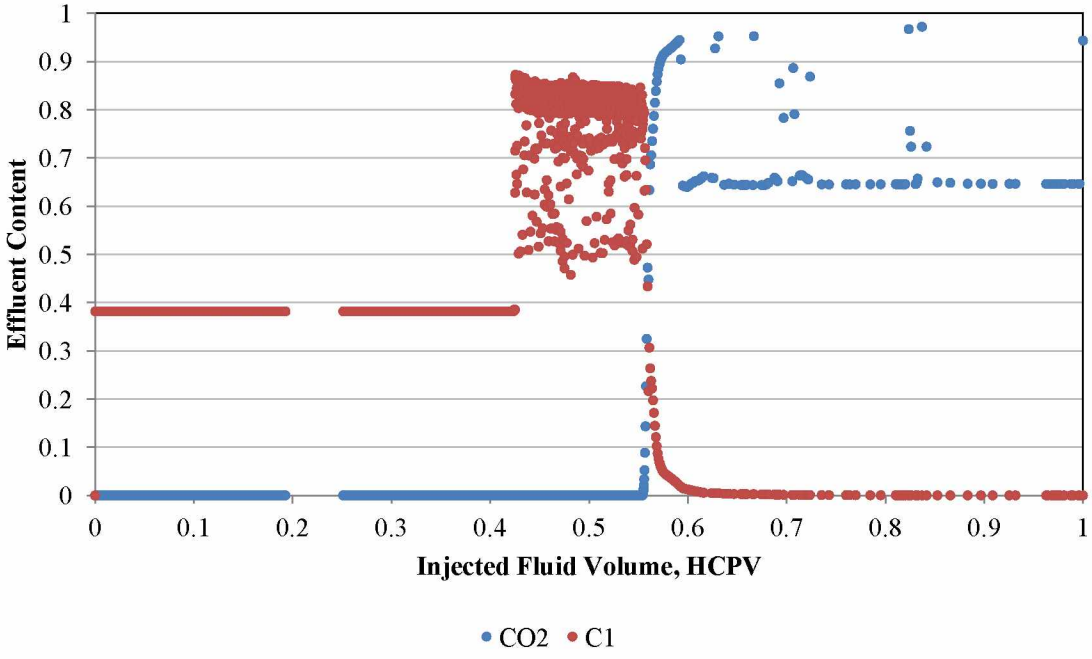

Figure 32: Effluent CO_2 and C_1 content of produced oil and gas

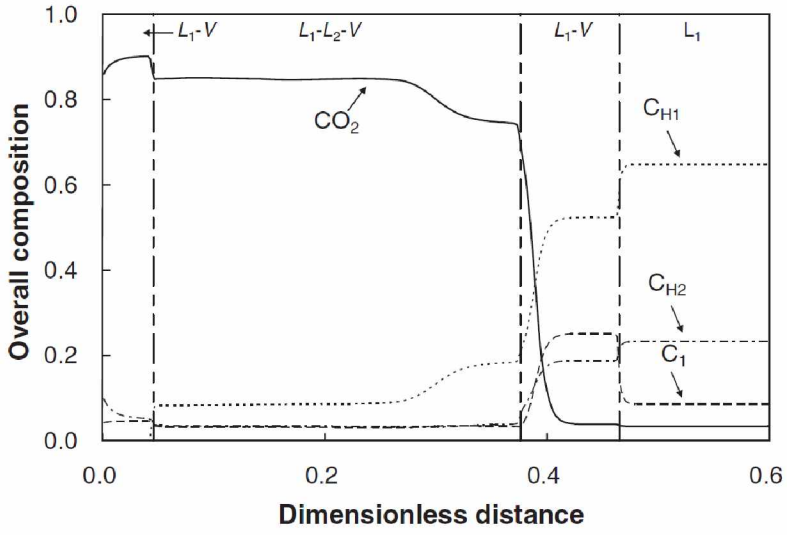

Figure 33: Overall composition profile after 0.5 HCPV CO_2 injection (Okuno et al., 2011)

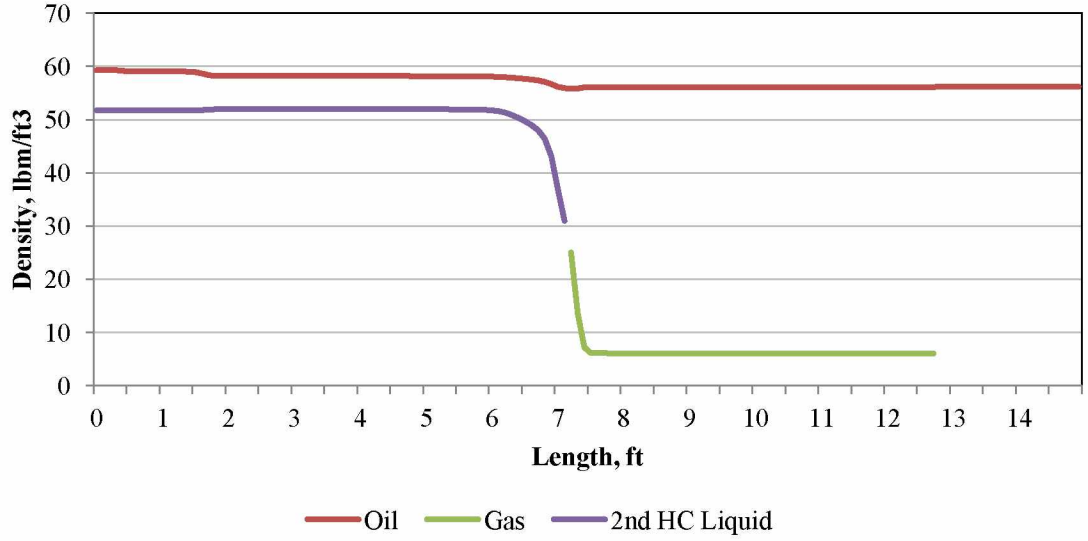

Figure 34: Density of oil, gas, and 2nd HC liquid phase after injecting 0.4 HCPV water and CO_2

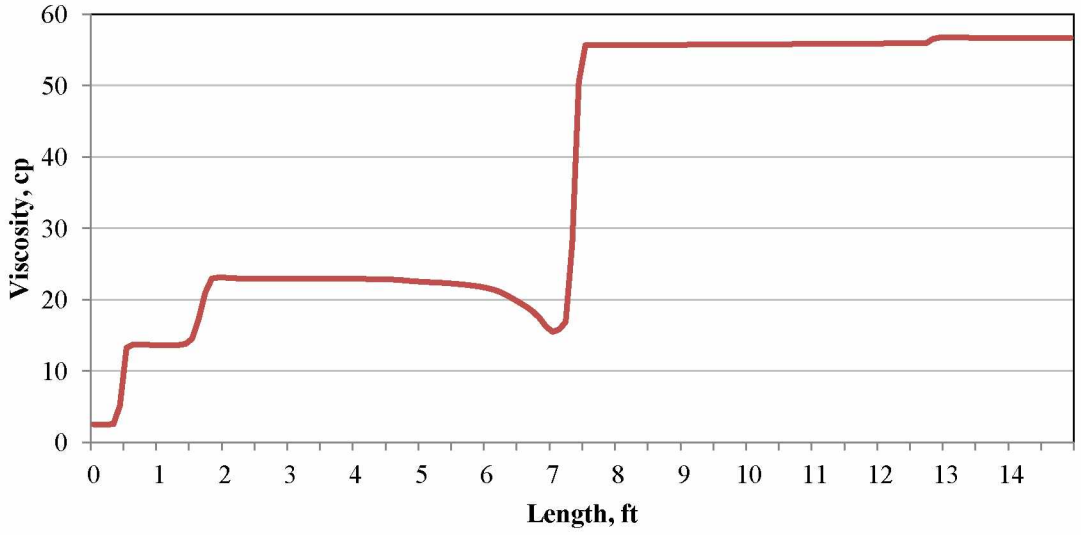

Figure 35: Viscosity of oil at 0.4 HCPV injected water and CO_2

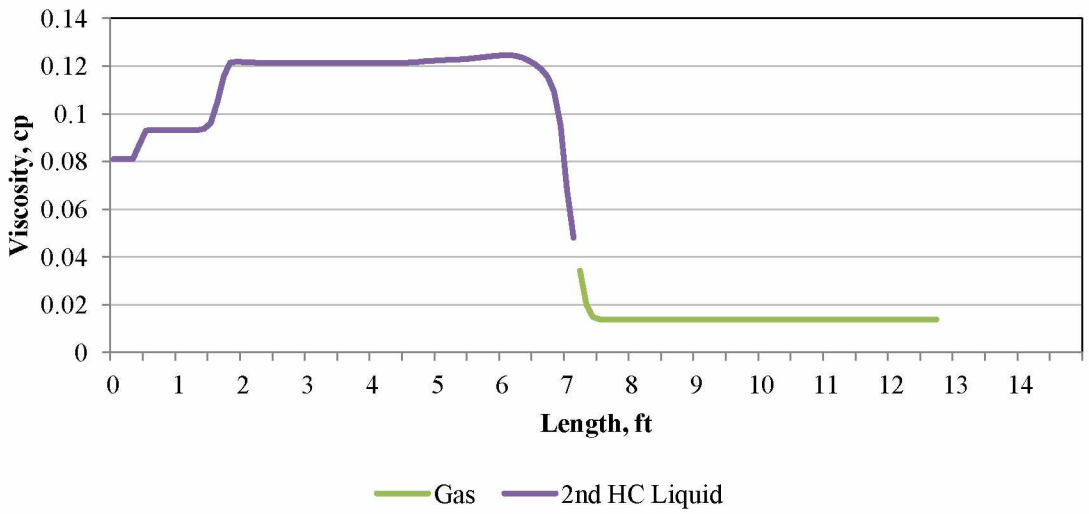

Figure 36: Viscosity of gas and second HC liquid at 0.4 HCPV injected water and CO_2

4.2.2 The 3D Pattern Model

In the 3D pattern model, waterflooding only recovered about 14% OOIP, and a large amount of oil was left unproduced. CO_2 WAG injection was simulated using the 3D pattern model in order to evaluate CO_2 injection performance in a heterogeneous model of the West Sak reservoir.

Figure 37 shows the oil viscosity in the 3D pattern model at the beginning and end of CO_2 WAG injection. It shows that viscosity is decreased in the areas near the injection well. The results indicated that injected CO_2 mixed with the residual oil. Some CO_2 dissolved into the oil and, similar to 1D case, reduced the oil viscosity.

Oil viscosity is increased in the areas near the production well (Figure 37). The results indicate that the dissolved gas comes out of the reservoir oil, due to lower pressures in areas near the production well. The oil viscosity increases consequently (see Figure 15).

Figure 38 shows the oil saturation in 3D pattern model at the beginning and end of CO_2 WAG injection. The CO_2 was injected into the perforated layers, sand D, B and A2. It

displaced the reservoir oil and reduced the oil saturation in these layers. Some changes can be seen in the oil saturation of other layers.

Figure 39 shows waterflood and CO_2 WAG injection oil recovery in 3D pattern model. Total oil recovery, after injecting 1 HCPV water and CO_2, reaches about 18.5% OOIP. In other words, injecting CO_2 increased oil recovery by 4.5% OOIP over waterflooding oil recovery. This incremental oil recovery is equal to 112 million barrels of oil when it is scaled up to WSCA.

Figure 40 shows the sequestered CO_2 volume during CO_2 WAG injection into the 3D pattern model. Sequestered CO_2 volume is increased significantly during injection of CO_2 slugs. In second WAG cycle, injected water swept out some of CO_2 and reduced the sequestered volume. This phenomenon is more severe in the third WAG cycle. Total sequestered CO_2 reached about 1300 MMSCF after injecting 1 HCPV water and CO_2. This corresponds to 0.104 metric tons of sequestered CO_2 per barrel of produced oil.

If the results of the pattern model were scaled up, an estimated 48 million metric tons of CO_2 could be sequestered in the WSCA. This number appears reasonable when compared to the estimated CO_2 storage capacity of Schrader Bluff, a similar low-temperature reservoir in ANS with 2 billion barrels of OOIP and a reported CO_2 storage capacity of about 30 million metric tons (McKean et al.,1999).

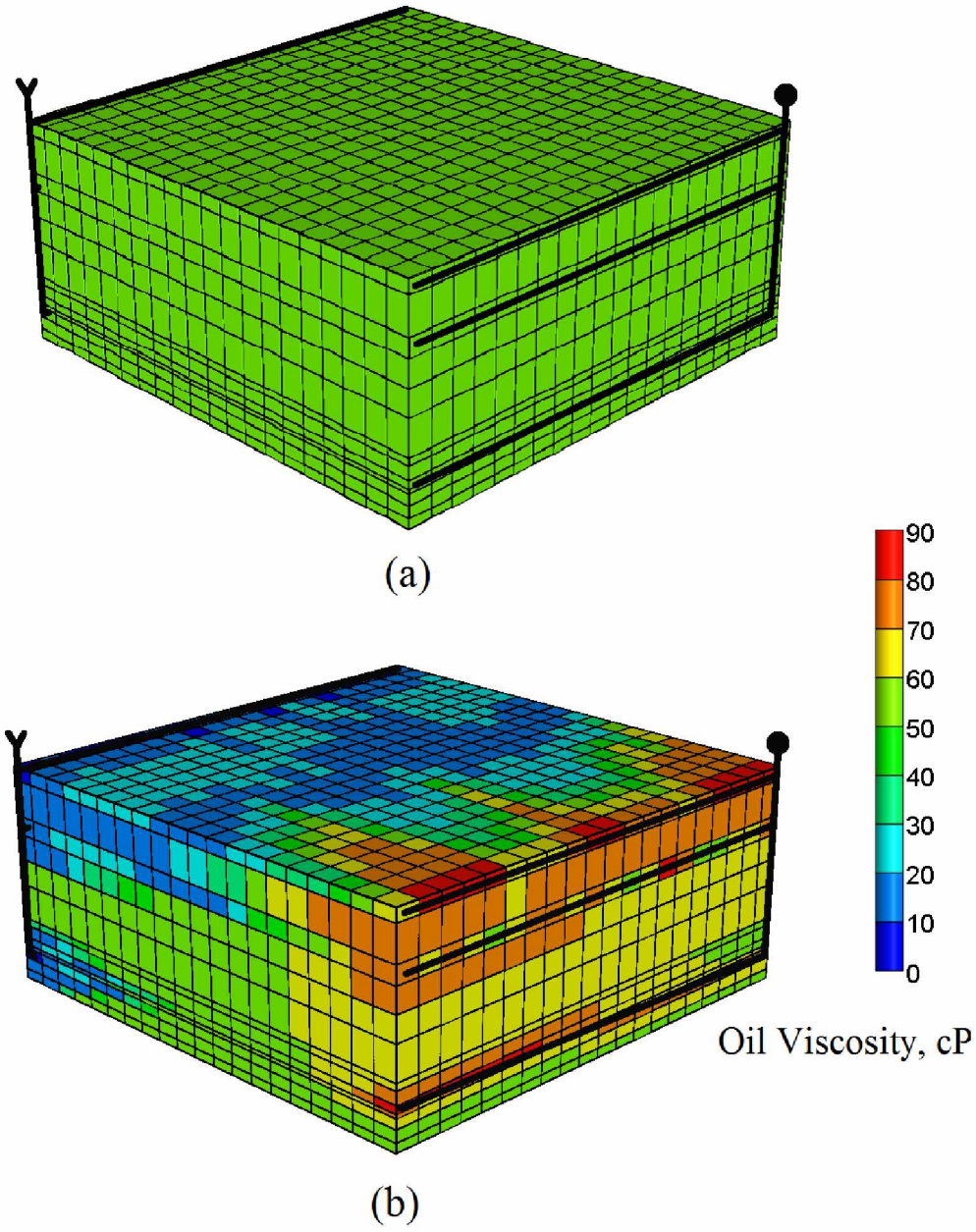

Figure 37: Oil viscosity at 0 HCPV (a) and 1 HCPV (b) CO_2 and water injection

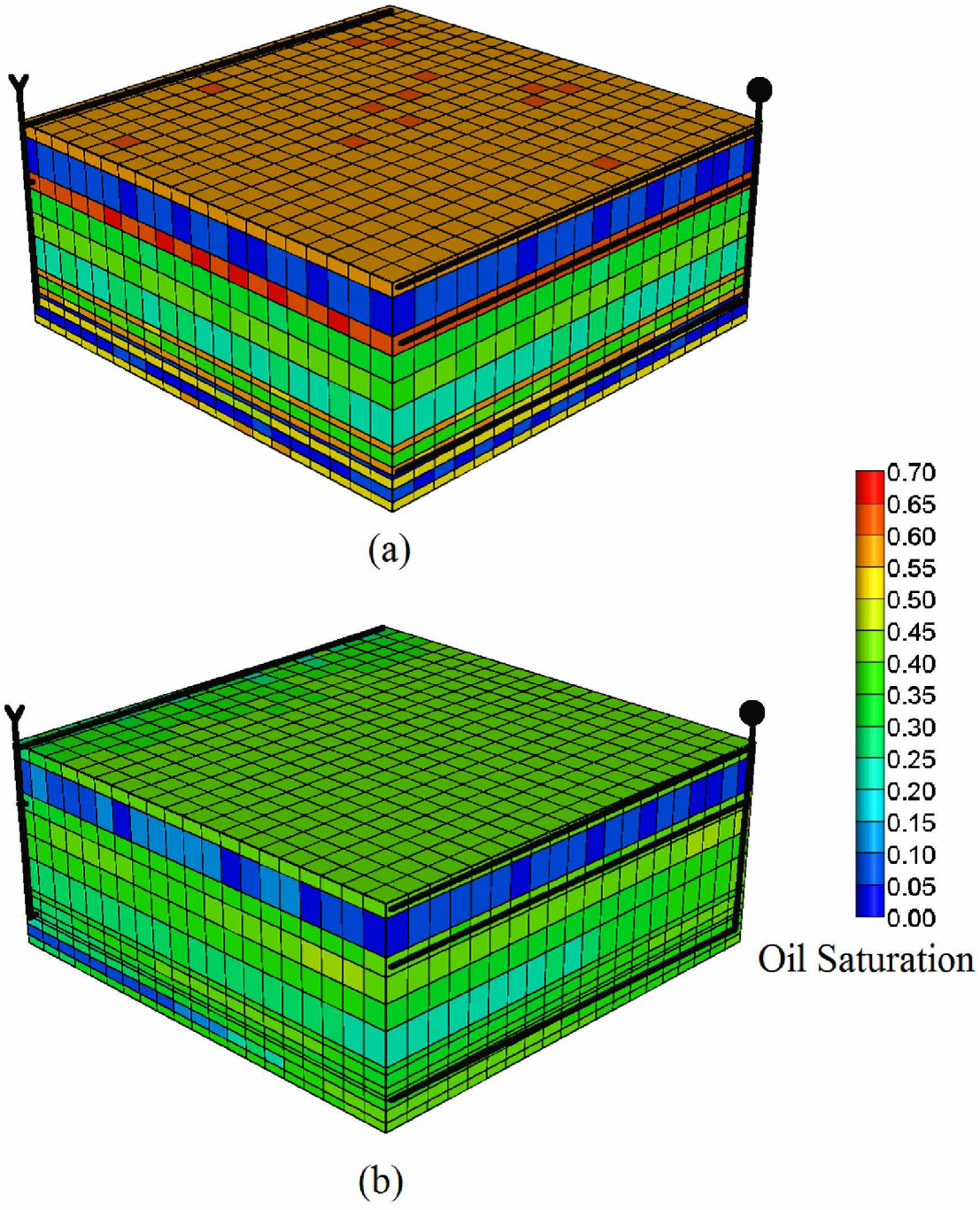

Figure 38: Oil saturation at 0 HCPV (a) and 1 HCPV (b) CO_2 and water injection

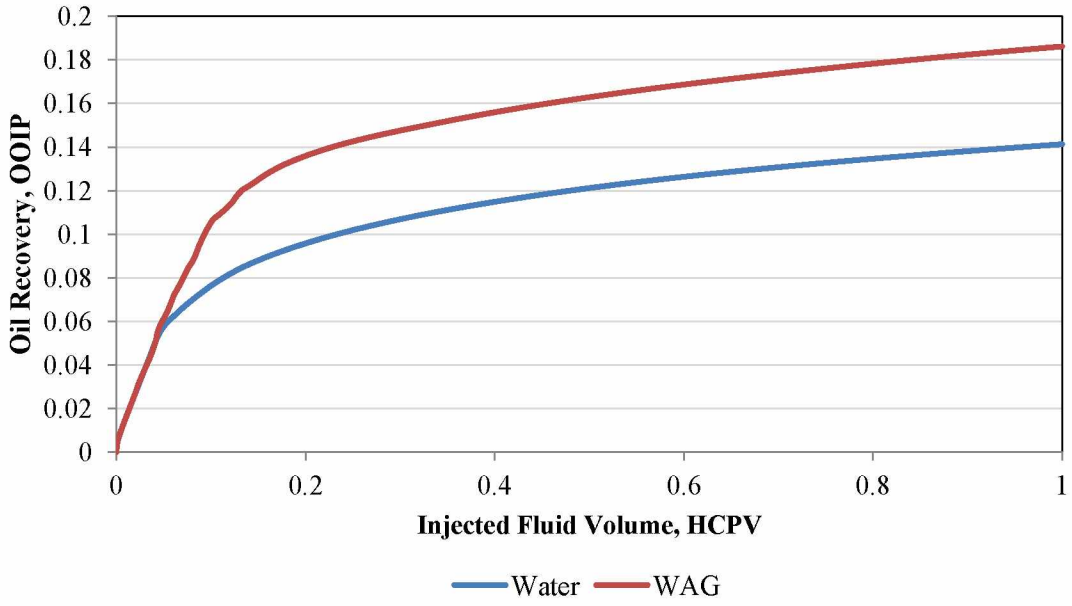

Figure 39: Oil recovery due to waterflooding and CO_2 injection

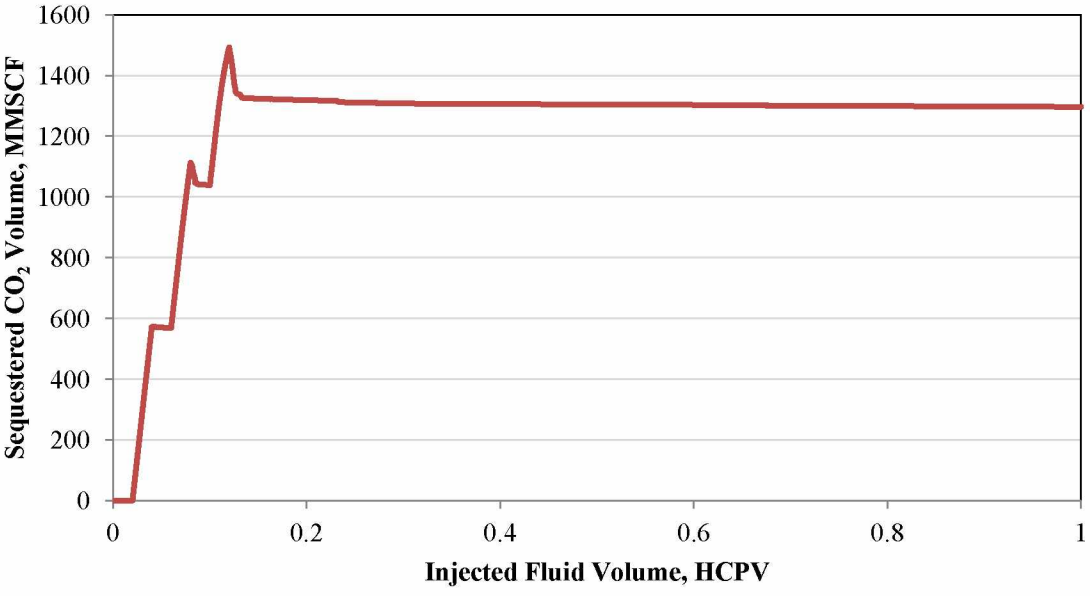

Figure 40: Sequestered CO_2 volume in the pattern model

Figure 41 shows total CO_2 concentration of hydrocarbon phases in the 3D pattern model. It shows that CO_2 was mainly injected into the sand D and B. This is probably due to better quality reservoir rocks.

A smaller amount of CO_2 was sequestered in sand A2 and adjacent layers. CO_2 did not contact the residual oil for the most part. This prevented the viscosity reduction mechanism in sand A2 that in turn lowered oil recovery due to CO_2 injection in the 3D pattern model.

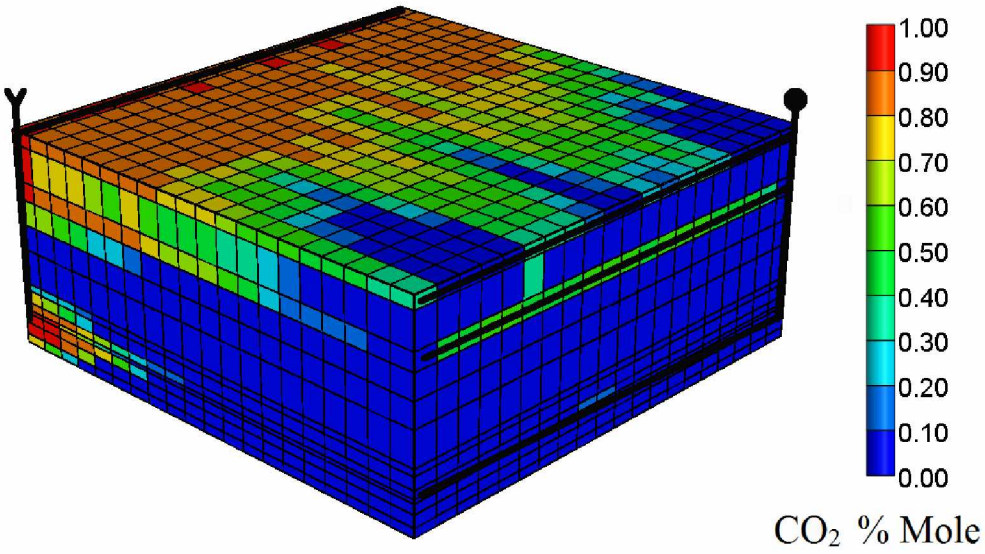

Figure 41: Concentration of CO_2 after 1 HCPV CO_2 and water injection

CO_2-oil mixtures can form L, L/V, L/L and L/L/V equilibriums at different pressures and CO_2 concentrations (see Figure 18). Figure 42 shows these phase equilibriums in 3D pattern model after injecting 0.12 HCPV water and CO_2. The figure indicates that in low-pressure areas around the production well, the mixture formed L/V equilibriums, while in high pressure areas near the injection well, they formed L/L equilibriums. In areas where CO_2 concentration was very low, below 0.10 mol%, only oil (L) phase was present. In some points, L/L/V was observed.

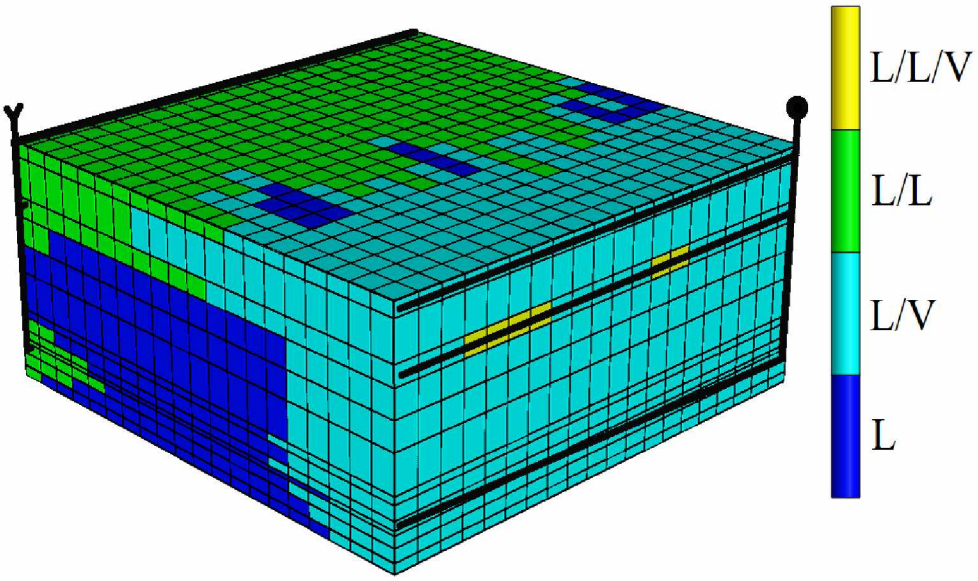

Figure 42: Phase distribution in 3D pattern model after 0.12 HCPV water and CO_2 injection

Formation of the second HC liquid phase has two important effects. First, the second HC liquid phase has lower relative permeability (at the same saturation) and higher viscosity compared to the gas phase. Therefore, mobility of second HC liquid phase is lower than the mobility of gas phase. This lower mobility improves the conformance in areas near the injection well, improving the sweep efficiency and thus oil recovery. Second, the density of second HC liquid phase is significantly higher than the density of the gas phase. This means that a higher amount of CO_2 is sequestered in the same reservoir volume, due to formation of a second HC liquid phase.

Figures 43 and 44 show the gas and second HC liquid phase saturation after 1 HCPV water and CO_2 injection. The CO_2-oil mixtures in Figure 42 when flooded with water left a trapped gas phase near the production well (Figure 43) and trapped a second HC liquid phase near the injection well (Figure 44).

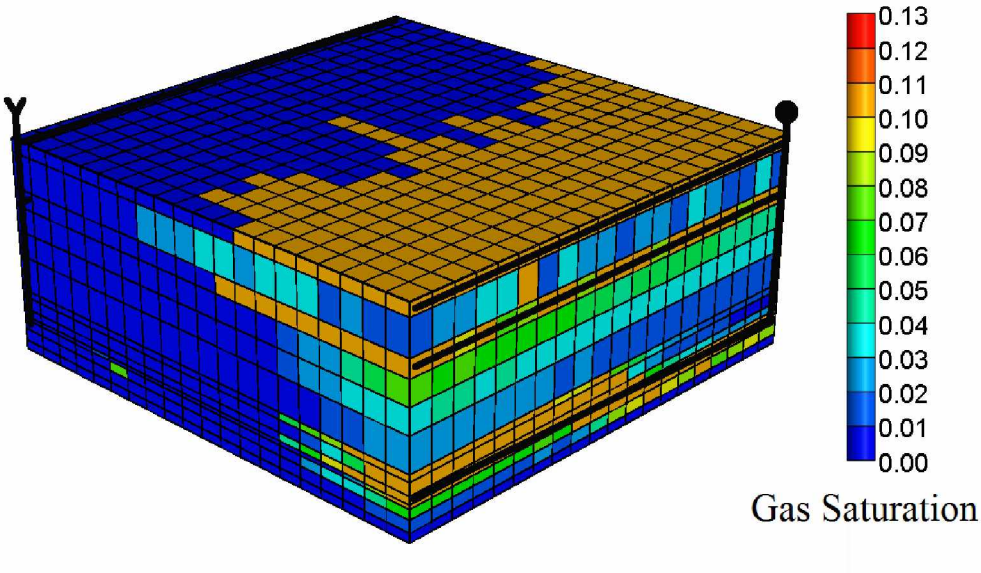

Figure 43: Gas saturation after 1 HCPV CO_2 and water injection

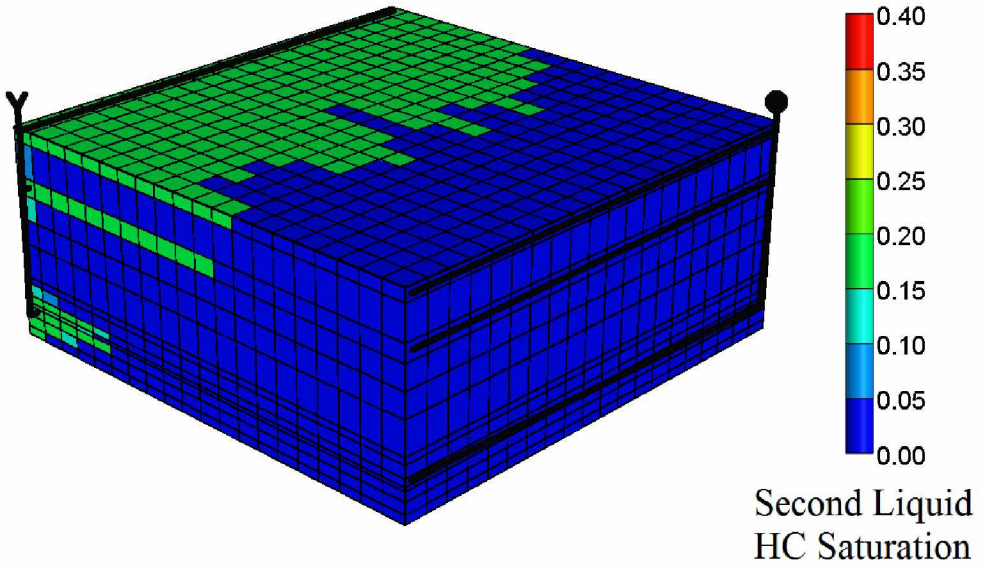

Figure 44: Second HC liquid saturation after 1 HCPV CO_2 and water injection

Figures 45–47 show the CO_2 concentration in oil, gas, and second HC liquid phases. In areas where CO_2 contacted oil phase, CO_2 dissolved in reservoir oil and sequestered there (Figure 45). CO_2 is also trapped in the gas and second HC liquid phases (Figures 46 and 47). Comparison of Figure 43 and Figure 46 reveals that the concentration of CO_2 is very low in some parts of the gas phase. These parts are most likely occupied by the front C_1 bank without being displaced by the following CO_2 bank.

Figure 48 shows the distribution of sequestered CO_2 volume in each phase. More than half of the sequestered CO_2 is trapped in the second HC liquid phase, and 41% is trapped as dissolved CO_2 in the residual oil (Figure 48). A very small amount, 3%, is sequestered as trapped gaseous CO_2. Dissolution of CO_2 in water was ignored in this case; therefore, no CO_2 was dissolved in the aqueous phase.

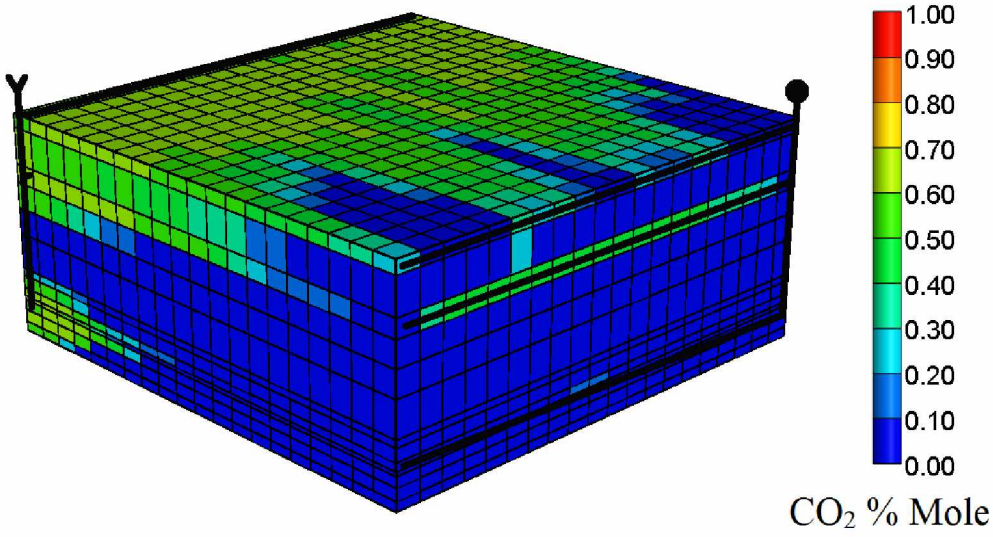

Figure 45: Concentration of CO_2 in oil phase after 1 HCPV CO_2 and water injection

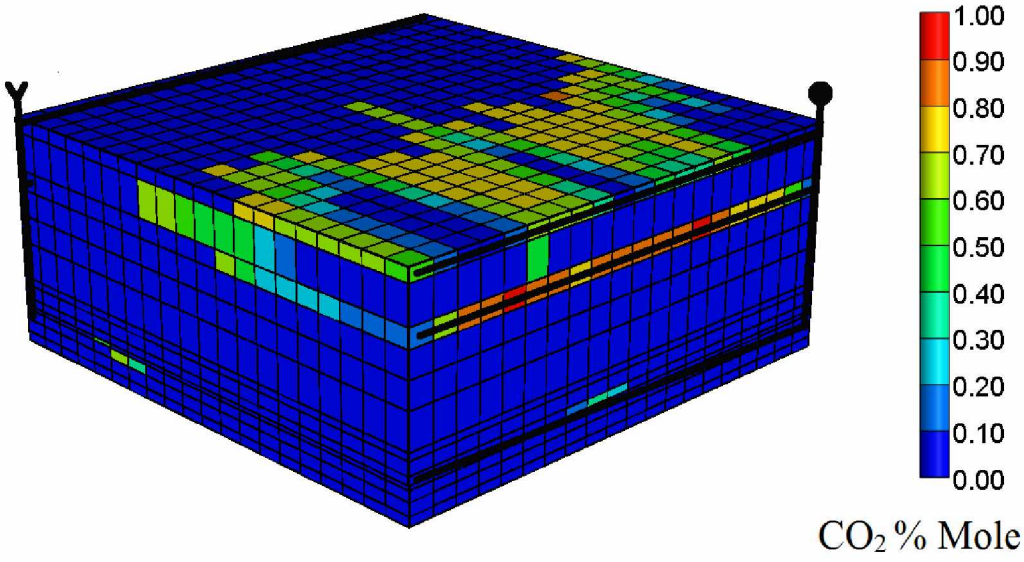

Figure 46: Concentration of CO_2 in gas phase after 1 HCPV CO_2 and water injection

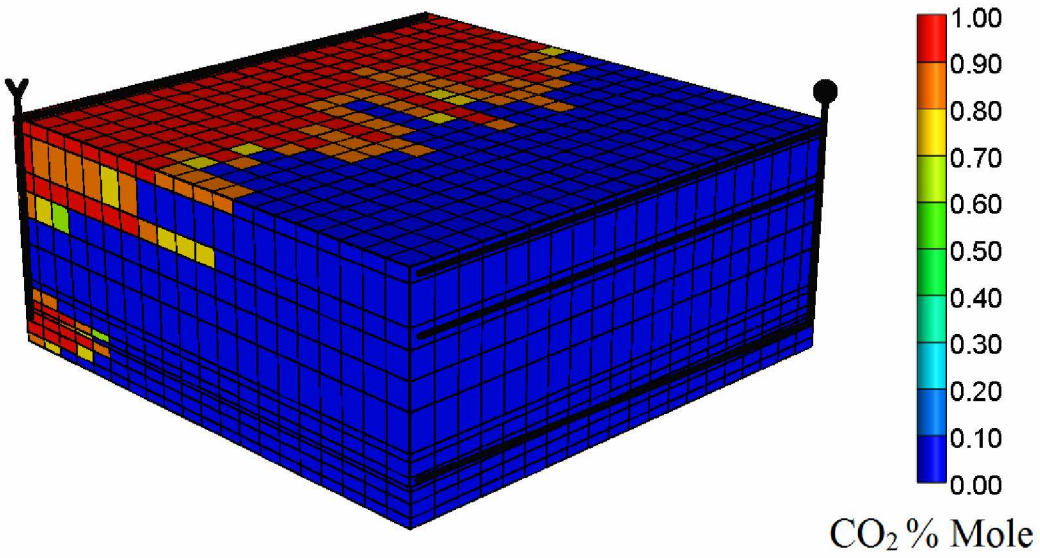

Figure 47: Concentration of CO_2 in second HC liquid phase after 1 HCPV CO_2 and water injection

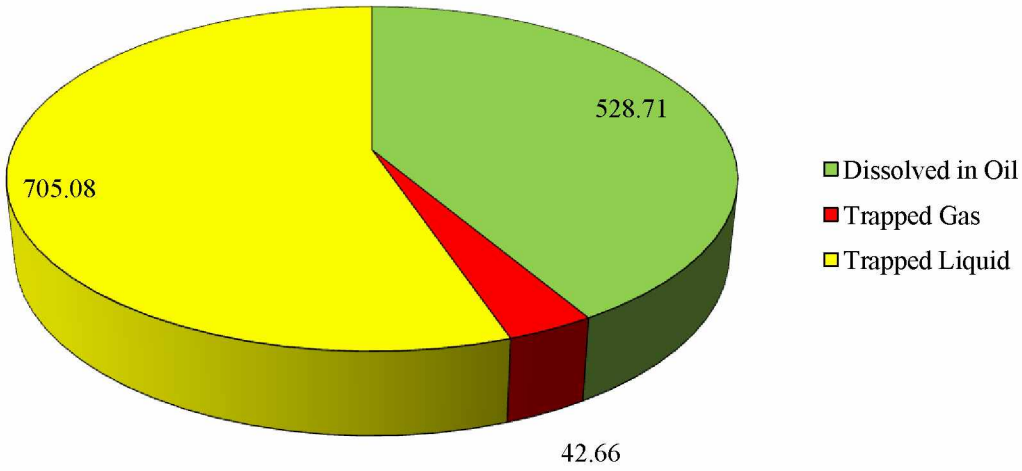

Figure 48: Sequestered CO_2 distribution (MSCF) in different reservoir fluids

4.3 Effect of Ignoring the Second HC Liquid Phase

One of the major questions in this project was the significance of accurate modeling of the CO_2 - oil complex phase behavior. To address this question, another 3D CO_2 -WAG case was defined. In this case, a two-phase flash calculation option was used instead of three-phase flash calculation. The total number of phases decreased to three by ignoring the second HC liquid phase.

Figure 49 shows that this simplification underestimates the oil recovery by about 0.8% OOIP. Although 0.8% difference in oil recovery is low, the estimated sequestered CO_2 volume is underestimated by 17% (Figure 50). These results show that using the simulators that are unable to handle four-phase flow for evaluation of CO_2 injection into a low temperature viscous oil reservoir like West Sak can lead to erroneous results.

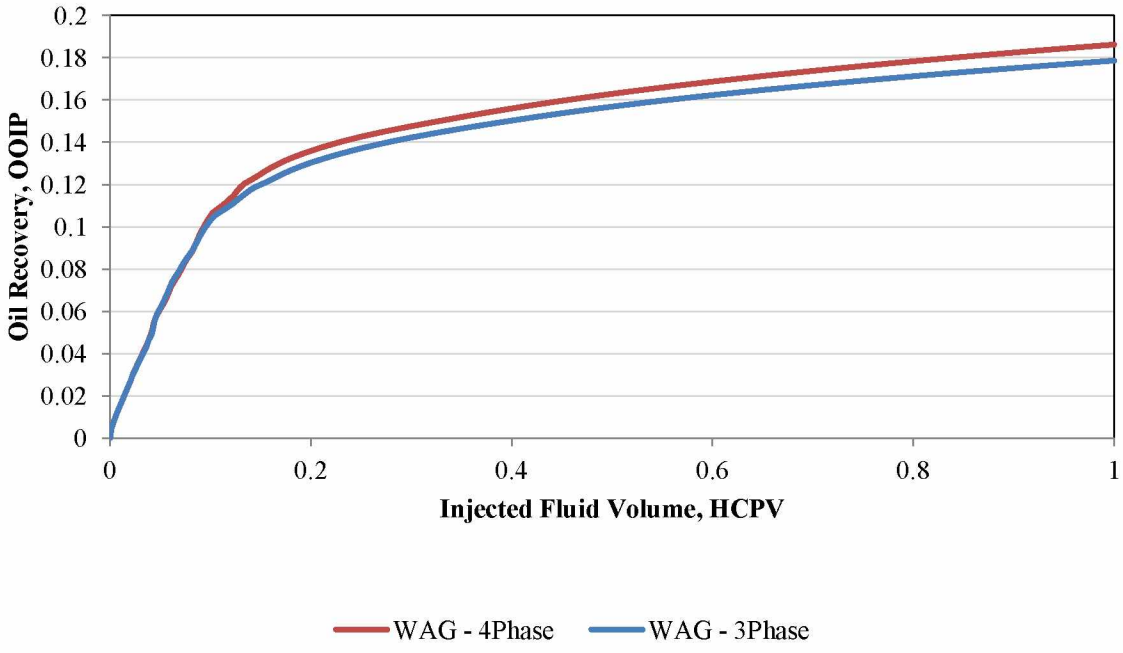

Figure 49: Oil Recovery for three- and four-phase flow simulation cases

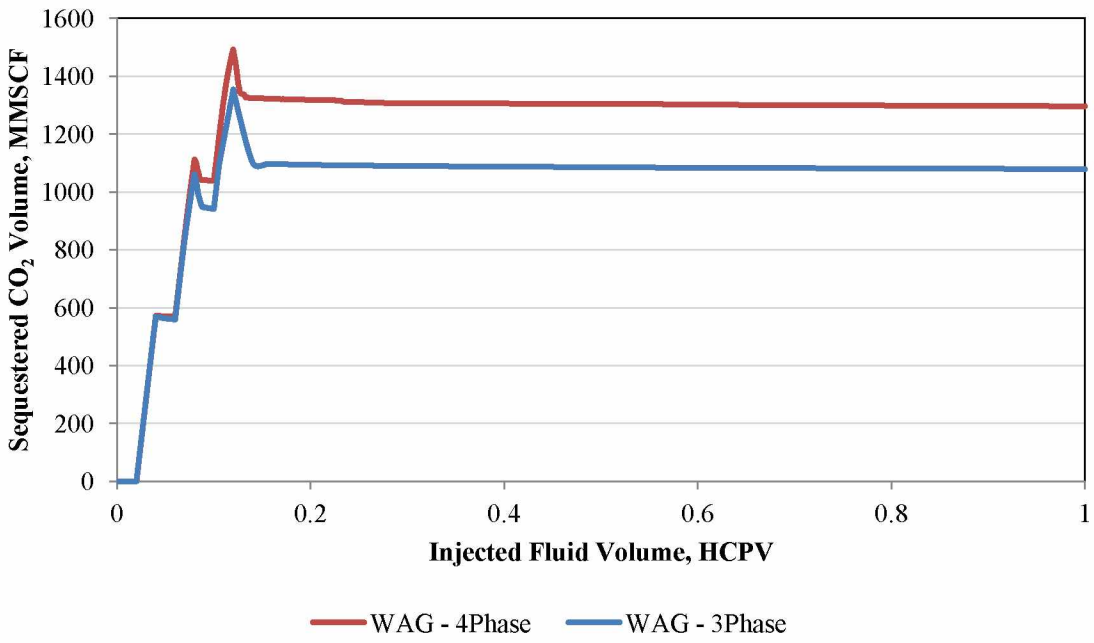

Figure 50: Sequestered CO_2 volume for three- and four-phase flow simulation cases

4.4 Effect of CO_2 Dissolution in Aqueous Phase

4.4.1 The 1D Model

Yan and Stenby (2010) suggested using 1D models to evaluate the effect of CO_2 dissolution in the water phase, before conducting the 3D simulation cases. The previously built 1D model was used and CO_2 aqueous dissolution option was enabled.

Figure 51 shows the effect of considering the CO_2 aqueous dissolution option on the oil recovery of 1D model compared to the base case of CO_2 injection without considering CO_2 aqueous dissolution option. The results almost match in the trend and the final oil recovery.

Figure 52 shows the effect of considering the CO_2 aqueous dissolution option on the sequestered CO_2 volume. The results are almost identical in trend until 0.56 HCPV is injected. After this point, the case in which CO_2 aqueous dissolution option is enabled shows slightly higher values about 5%, for sequestered CO_2 volume. It should be noted

that in this model injected CO_2 volume, 0.25 HCPV, is quite high compared to injected CO_2 volume, 0.06 HCPV, in the 3D model.

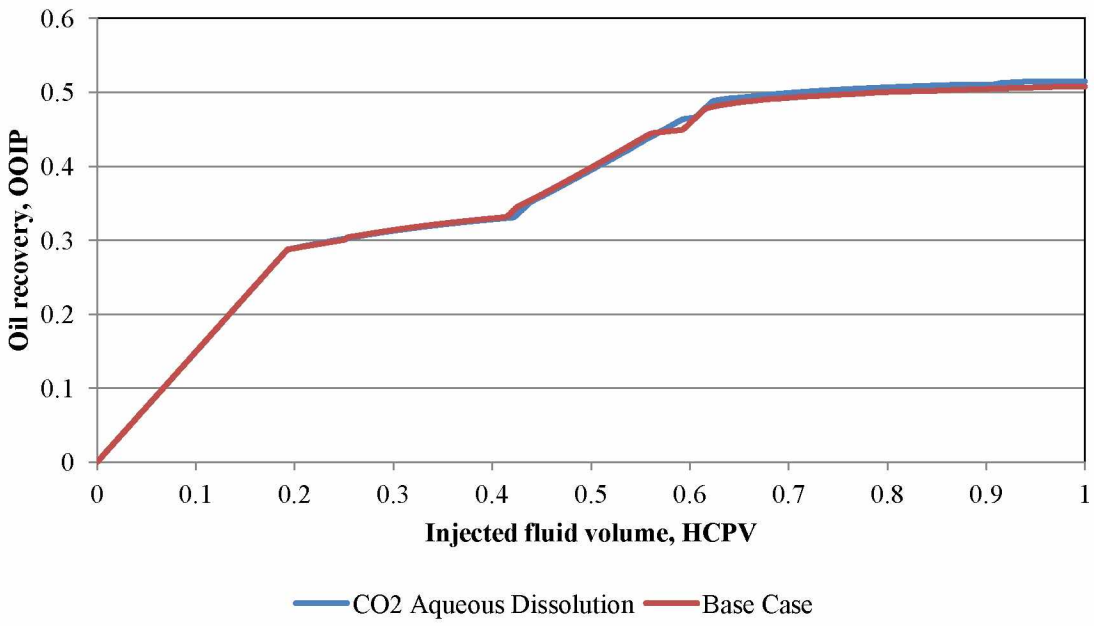

Figure 51: Effect of CO_2 aqueous dissolution option on oil recovery

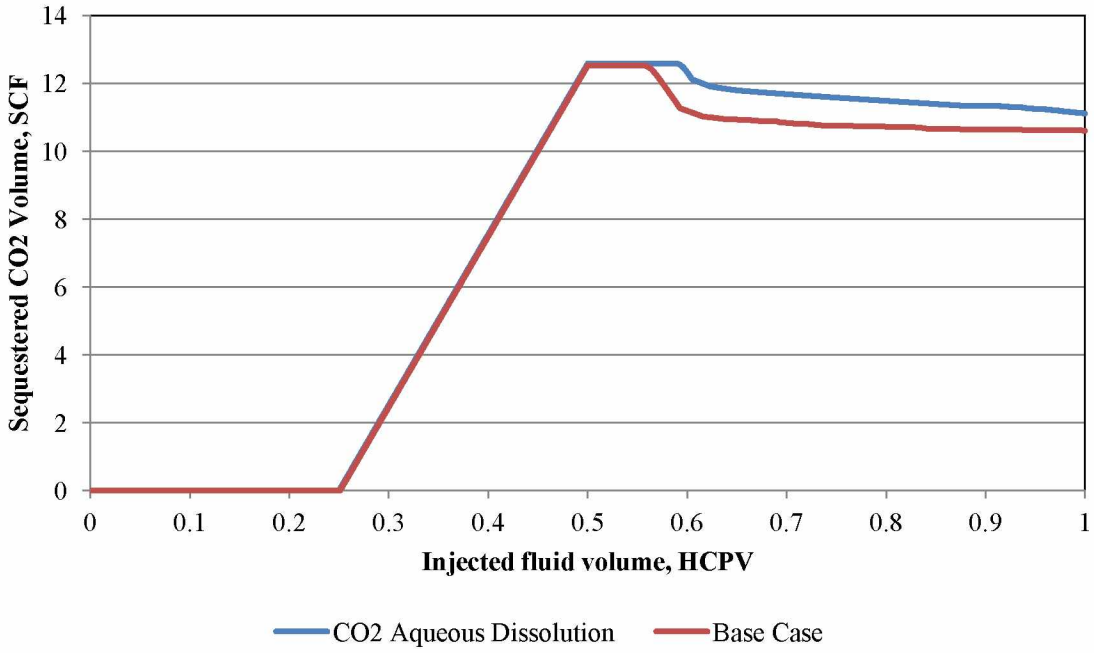

Figure 52: Effect of CO_2 aqueous dissolution option on sequestered CO_2 volume

4.4.2 The 2D Pattern Model

With the CO_2 aqueous dissolution option enabled in the 3D model, computational time of the simulation increased significantly. Therefore, a 2D Y-Z cross-section model was used to evaluate the significance of CO_2 dissolution in the aqueous phase. The results of 2D Y-Z model will be more representative than 1D models as it captures the vertical permeability variations of the reservoir.

The initial injection/production scheme, injecting 1.0 HCPV of CO_2 and water, caused convergence problems that in turn terminated the simulation run. So a CO_2 WAG process was simulated by injecting a 0.02 HCPV water slug followed by a 0.02 HCPV CO_2 slug. Water was then injected for a total CO_2-water injection of 1.0 HCPV. A similar case was defined and CO_2 aqueous dissolution option was included in the data file.

Minimal changes were observed in the oil recovery and sequestered CO_2 volume in the model compared to the 2D model case without CO_2 aqueous dissolution option (Figures 53–54). The oil recovery values are very similar to each other in trend and final values (Figure 53). Total sequestered CO_2 volume is equal in both cases (Figure 54).

Considering CO_2 aqueous dissolution option changed the sequestered CO_2 volume in 1D model, but it did not change total sequestered CO_2 volume in 2D model. This difference is possibly due to lower injected CO_2 volume in 2D model.

The distribution of the sequestered CO_2 in different reservoir fluids, however, changed significantly after considering CO_2 aqueous dissolution in aqueous phase (Figure 55). The result shows that about 19% of CO_2 is sequestered in water phase, after considering CO_2 aqueous dissolution in aqueous phase. Sequestered CO_2 volume in oil and second HC liquid phase decreased. The trapped CO_2 volume in the gas phase remained constant.

The overall results show that dissolution of CO_2 in aqueous phase can be safely ignored, as we are mainly interested in the oil recovery and sequestered CO_2 volumes.

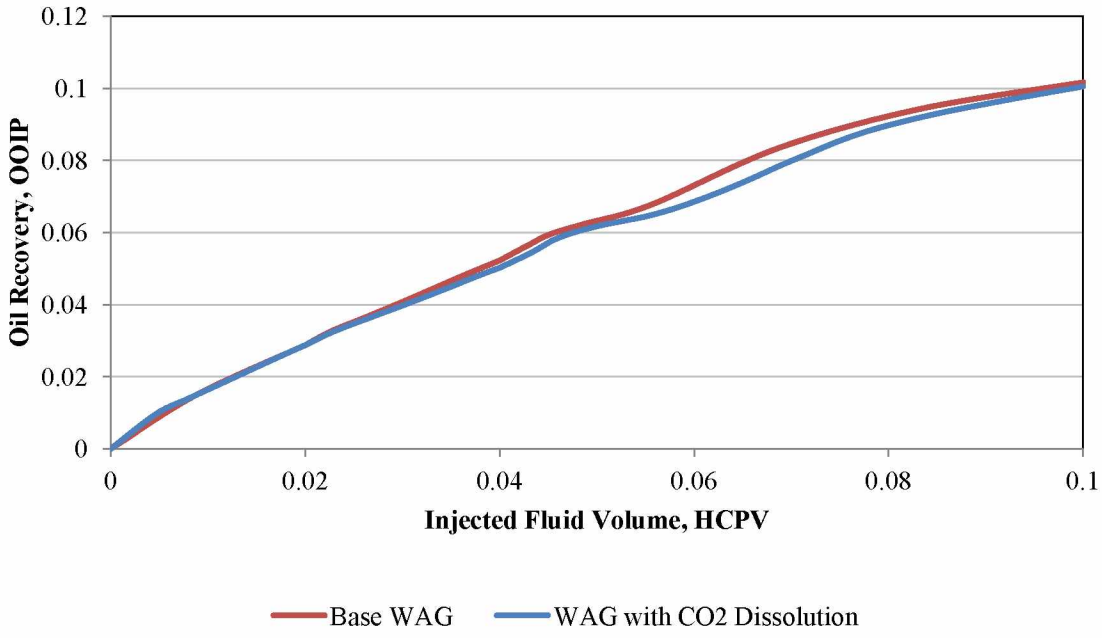

Figure 53: Effect of CO_2 aqueous dissolution option on oil recovery

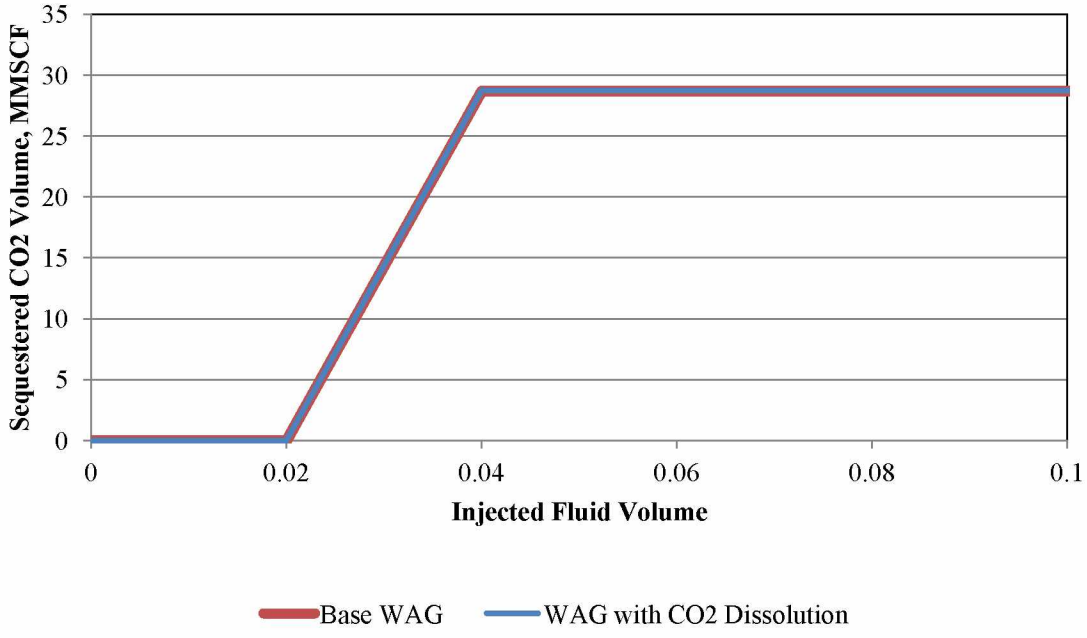

Figure 54: Effect of CO_2 aqueous dissolution on sequestered CO_2 volume

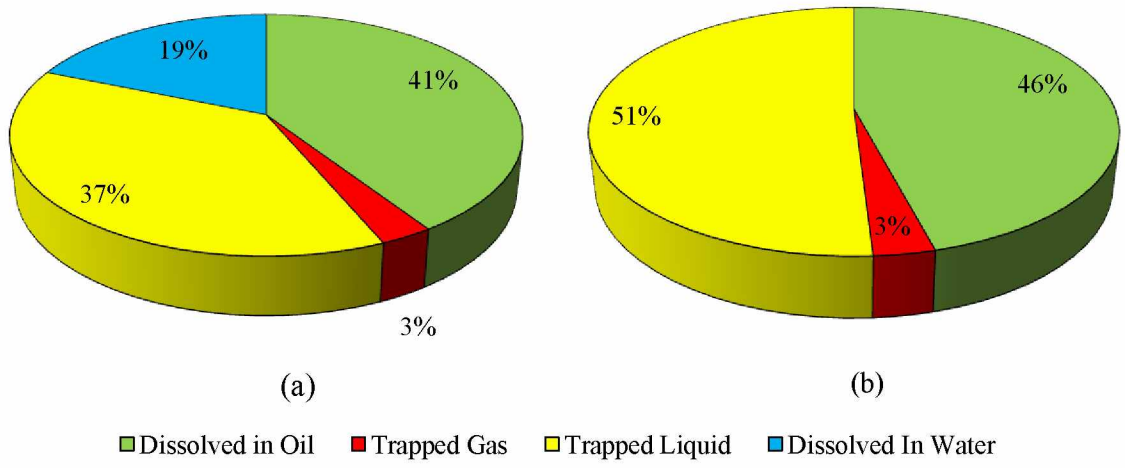

Figure 55: Sequestered CO_2 distribution in different phases with (a) and without (b) considering CO_2 dissolution in water phase

4.5 Effect of Enriching CO_2 with Natural Gas Liquid (NGL)

Enriching methane or CO_2 by mixing them with NGL is a common practice. This is thought to enhance solubility, viscosity reduction, and oil swelling mechanisms and lead to increased oil recovery (Stone and Crump, 1956). However, NGL mixtures are expensive and the cost of enrichment must be considered. Enrichment also can decrease the sequestered CO_2 volume, as the trapped gas/liquid will include components other than CO_2.

To simulate this, the average composition of Prudhoe Bay miscible injectant (MI) was mixed with CO_2 in different proportions (McGuire and Moritz, 1992) (Table 9). Similar to pure CO_2 case, a batch of three-phase flash calculation was conducted to generate the P-X plot for enriched CO_2- oil mixtures. The result showed that this enrichment changed the phase equilibrium boundaries for the enriched CO_2 and oil mixture (Figure 56).

Table 9: Average central gas facility MI composition

Components	CO_2	C_1	C_2	C_3	NC_4
Z	0.2115	0.3344	0.1978	0.2152	0.0404

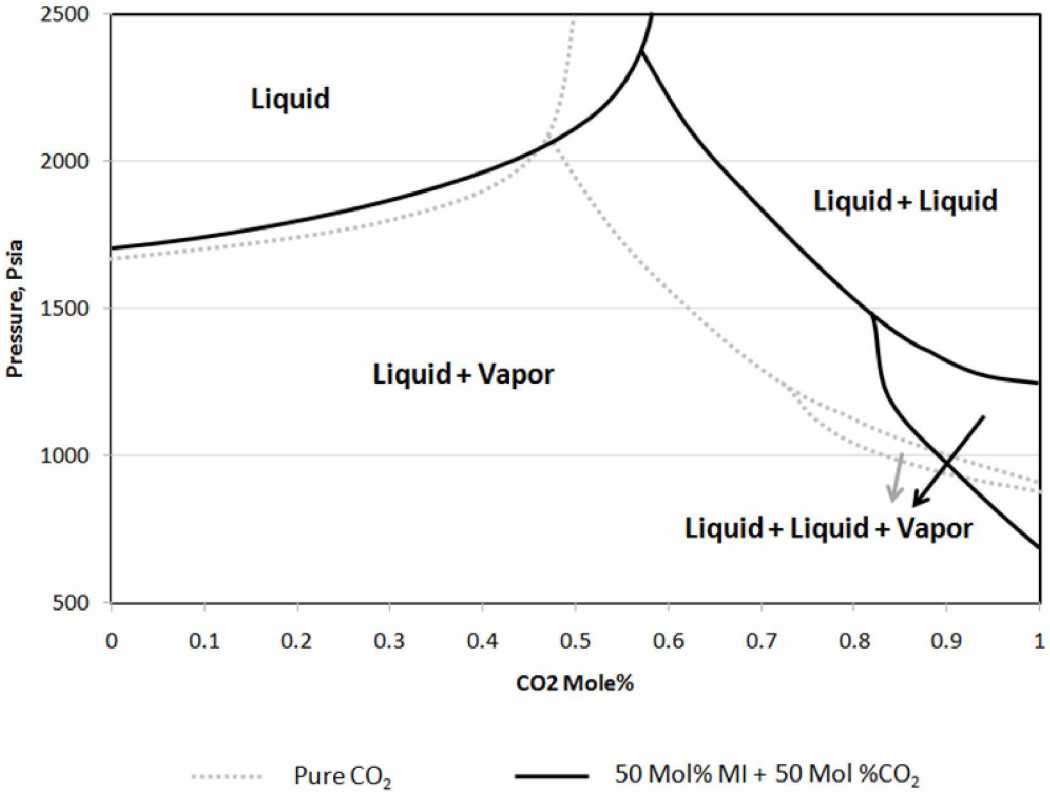

Figure 56: Effect of NGL enrichment on the simulated phase equilibrium boundaries

4.5.1 The 1D Model

CO_2 was mixed with different concentrations of the MI (10, 25, and 50 mol%). The mixture was injected into the sand B 1D model. The injection/production scheme was the same as in the pure CO_2 WAG case.

Figure 57 shows oil recovery for different concentrations of MI as compared to a base case of CO_2 injection with no NGL enrichment. When compared to pure CO_2 WAG, the oil recovery increased by 14% OOIP using CO_2 with 50 mol% MI.

Figure 58 shows sequestered CO_2 volume for different concentration of MI as compared to base case of CO_2 injection without NGL enrichment. It shows that the sequestered CO_2 volume decreased by mixing CO_2 with other components (Figure 58). This is due to lower amount of injected CO_2, when mixing CO_2 with MI.

The results indicate that injecting water, after pure CO_2 slug, sweeps out some of the injected CO_2. Therefore, the sequestered CO_2 volume decreases after 0.5 HCPV in pure CO_2 case (red line, Figure 58). This effect deceases with NGL enrichment of the CO_2 slug, possibly due to changing saturation profile for second HC liquid phase.

Despite the reduced sequestered CO_2 volume, the significantly increased oil recovery, seen in Figure 57, may be critical to the economy of the project.

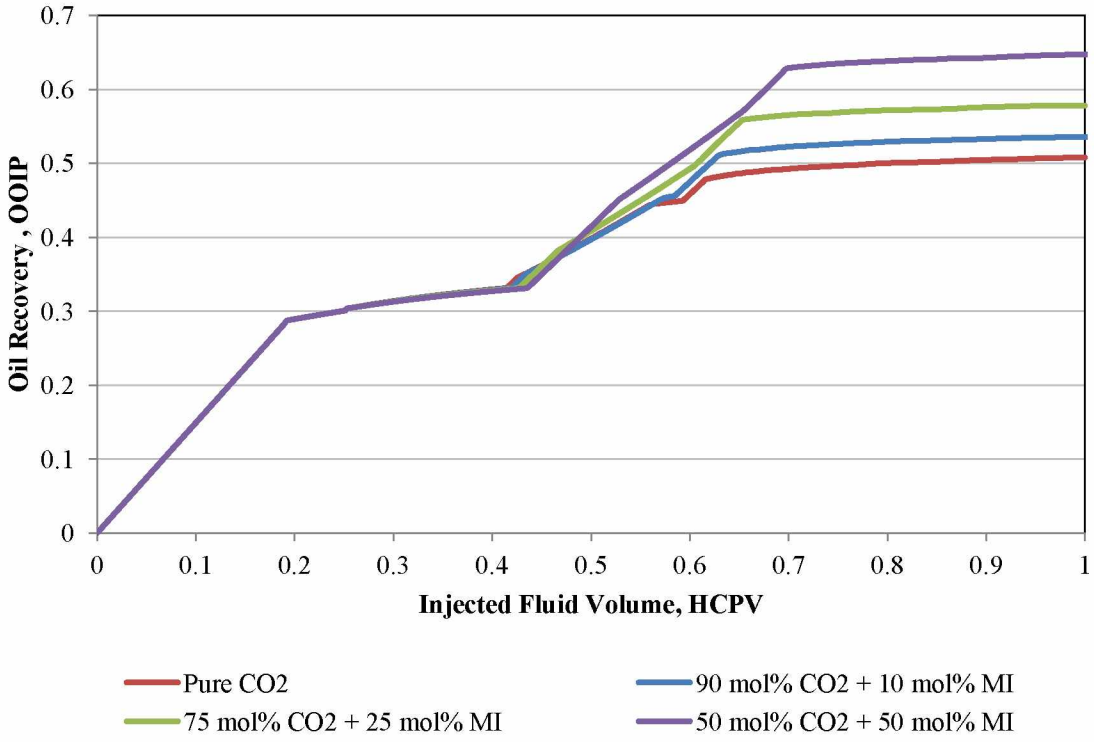

Figure 57: Effect of CO_2 NGL enrichment on oil recovery of sand B 1D model

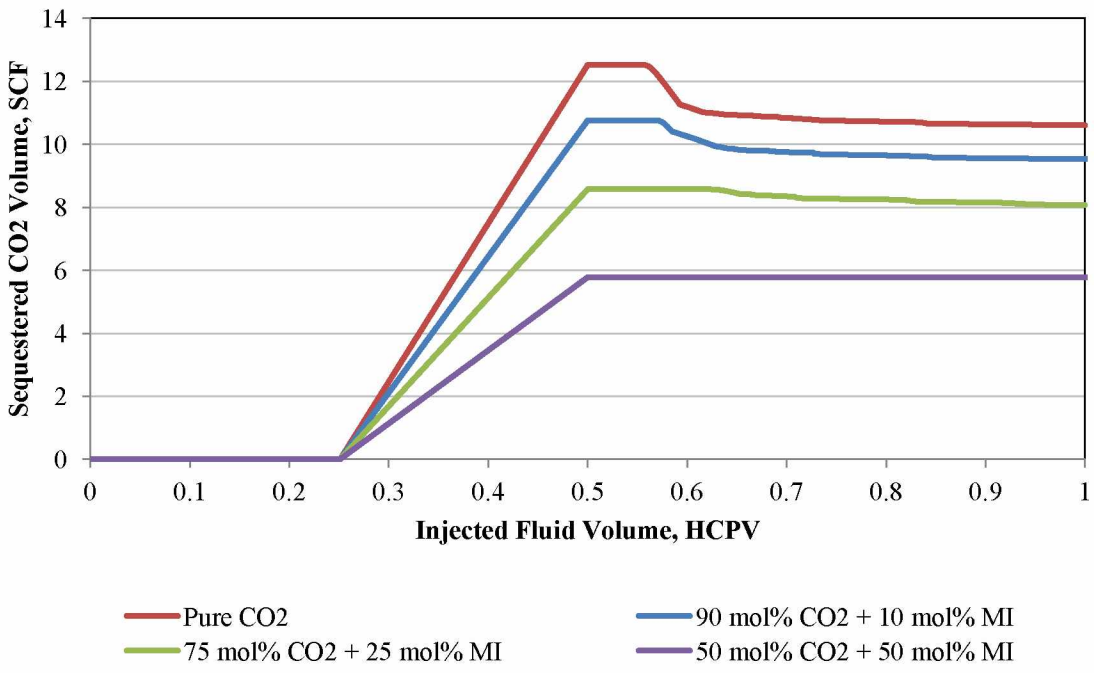

Figure 58: Effect of NGL enrichment on CO_2 sequestered volume in sand B 1D model

4.5.2 The 3D Pattern Model

The 1D model enrichment scheme was repeated in the 3D pattern model to evaluate the performance of NGL enrichment.

Figures 59 and 60 show the oil recovery and sequestered CO_2 volume for pure CO_2 and different concentration of CO_2-MI. Oil recovery changed only slightly, but sequestered CO_2 volume decreased significantly. Sequestered CO_2 volume is increased significantly during injection of CO_2/MI slugs. In second WAG cycle, injected water swept out some of CO_2/MI and reduced the sequestered volume. This phenomenon is more severe in the third WAG cycle. The sequestered CO_2 volumes decrease with increasing MI mol% in injectant.

Although the 1D model result for NGL enrichment was promising, enrichment of CO_2 is a less efficient option in the West Sak reservoir since NGL enrichment decreased sequestered CO_2 volume without significantly increasing incremental oil recovery. The

difference in results of 1D and 3D model is possibly due to low injected mixture, 0.06 HCPV, in 3D pattern model.

Regardless of cost increase, enrichment decreased the sequestered CO_2 volume by 44% in the 50 mol% CO_2 and 50 mol% MI case, without significant increase in oil recovery.

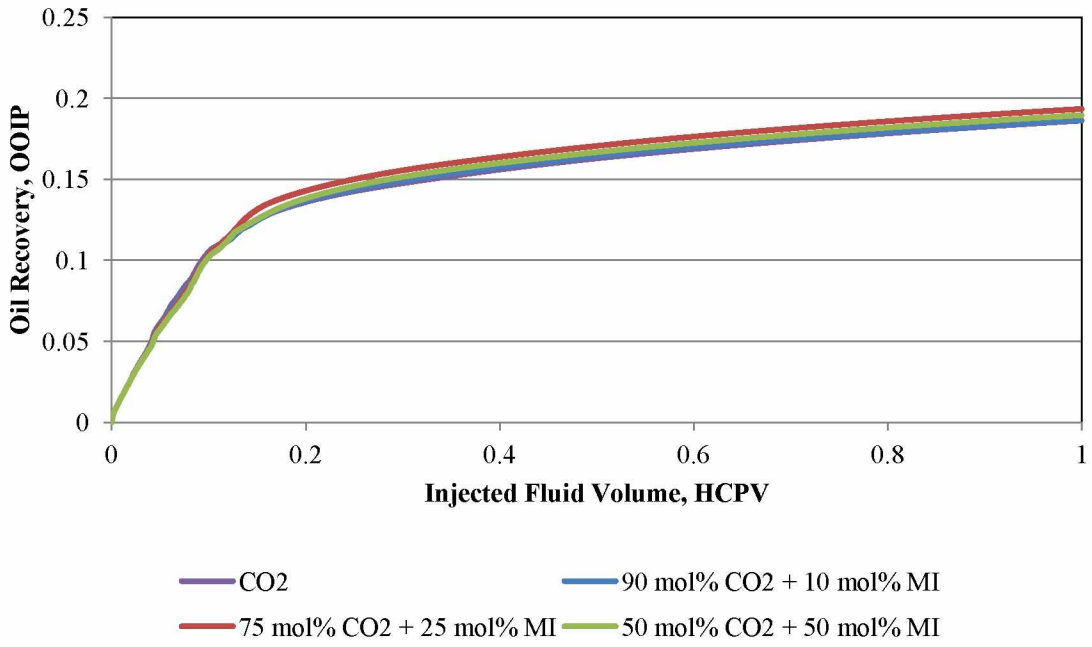

Figure 59: Effect of enrichment on oil recovery

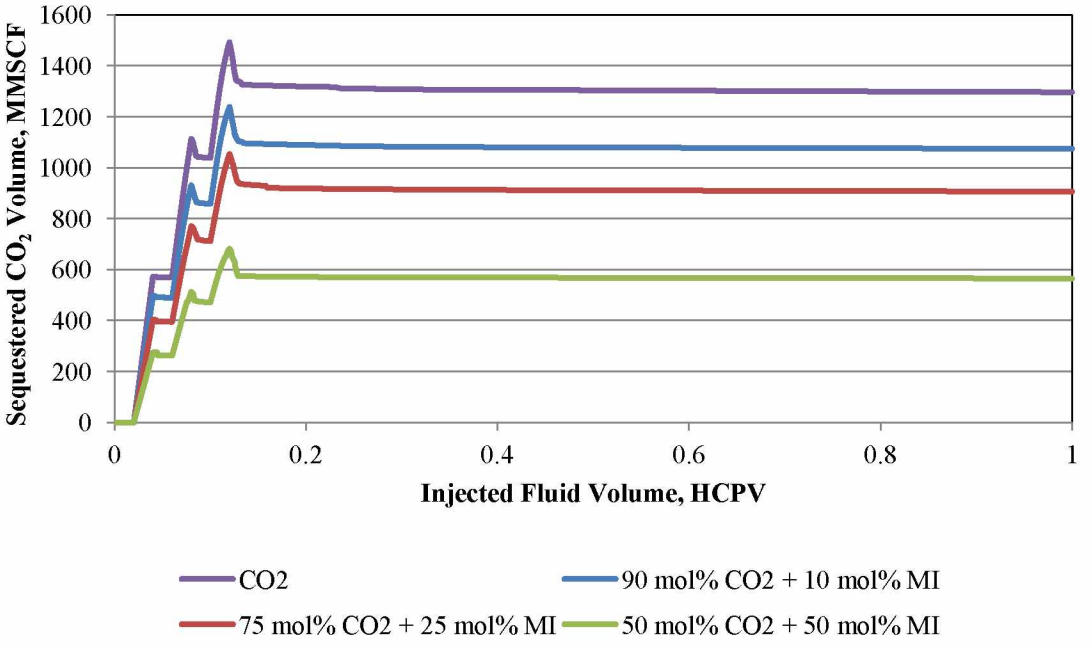

Figure 60: Effect of NGL enrichment on sequestered CO_2 volume

4.6 WAG Parameters

Due to the high mobility of CO_2, viscous fingering can occur in the field and cause early breakthrough. The ratio of injected gas volume to water volume (WAG ratio) and volume of each injected slug (slug size) can increase the sweep efficiency to some degree (Caudle and Dyes, 1958), resulting in increased oil recovery and increased sequestered CO_2 volume.

Sensitivity of the simulation results to WAG ratio and slug size was evaluated in the 3D pattern model. Table 10 shows WAG parameters for the simulation cases. Results of the simulations are shown in Figures 61 and 62. Oil recovery values were affected slightly as these parameters varied (Figure 61). Sequestered CO_2 volumes were slightly higher for the cases with 0.02 HCPV (Figure 62), showing that small slugs can slightly increase sequestered CO_2 volume. These slight differences shows that sweep efficiencies did not change significantly in these cases. The result indicates that the injecting CO_2 WAG in different WAG ratios and slug sizes does not affect the final oil recovery and sequestered CO_2 volume.

Table 10: WAG flooding parameters

Case Number	WAG ratio	Slug size (HCPV)
1	0.5	0.02
2	1	0.02
3	2	0.02
4	0.5	0.03
5	1	0.03
6	2	0.03

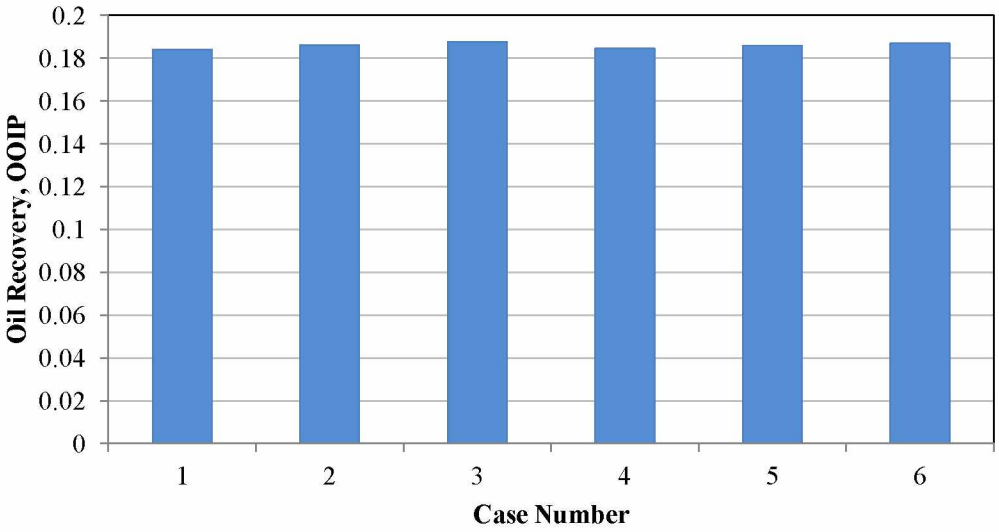

Figure 61: Effect of WAG parameters on oil recovery

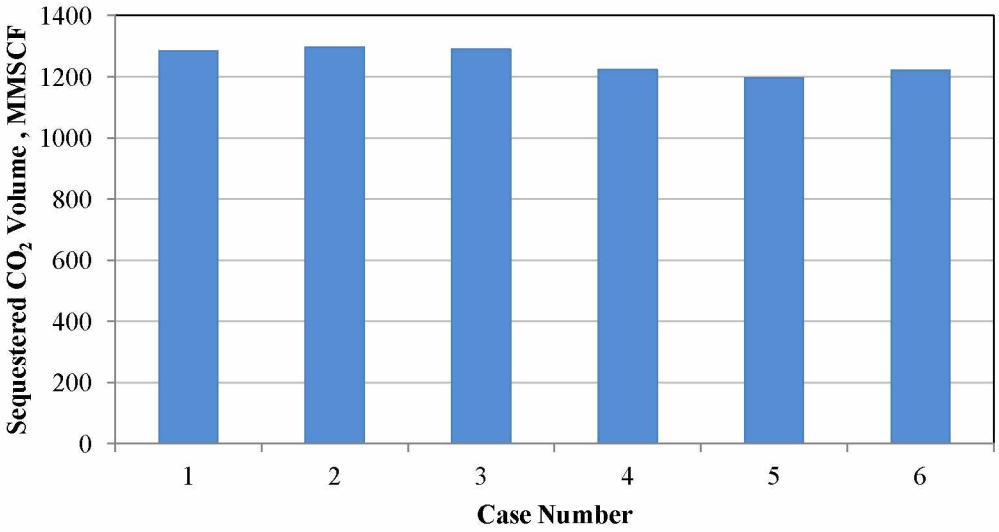

Figure 62: Effect of WAG parameters on sequestered CO_2 volume

Chapter Five: Conclusions and Recommendations

5.1 Conclusions

A large amount of residual oil was left in the West Sak reservoir 3D pattern model after waterflooding. The results of the 1D model cases for each layer showed oil recovery factor in the range of 0.27–0.39 OOIP for 1 HCPV of water injection. The 3D pattern showed that final oil recovery after injection of 1 HCPV water was only 14% OOIP. The difference was due to low volumetric sweep efficiency, lack of perforation in sand A1, A3, and A4 layers, and also higher permeability and thickness of sands D and B compared to sand A2.

When CO_2 was injected into the reservoir and displaced the oil, two simultaneous mechanisms occurred in the displacing front. While CO_2 dissolved in the oil, C_1 and intermediate components vaporized into a CO_2-rich phase. Part of the vaporized C_1 formed a separate gas phase ahead of the CO_2 bank. Due to this displacement and dissolution of CO_2 in the oil phase, in 1D models the oil recovery increased by 15% OOIP, compared to the waterflooding case. Due to layering in the reservoir, the increased oil recovery was only 4.5% OOIP in the 3D pattern model. This translates to 112 million barrels of oil production when multiplied by WSCA OOIP. The results also showed that 0.104 metric tons of CO_2 would be sequestered for production of one barrel of oil. Extending these results to the whole reservoir, an estimated 48 million metric tons of CO_2 would be sequestered in WSCA.

Due to low reservoir temperature in WSCA, a mixture of CO_2 and oil can form complex multi-liquid equilibriums. Results from the 3D CO_2-WAG case showed that ignoring this complex phase behavior could result in underestimation of the increased oil recovery by 0.8% OOIP and underestimation of the sequestered CO_2 volume by 17%. Therefore, a simulator capable of handling four-phase flow is required for accurate evaluation of CO_2 sequestration in West Sak and similar low-temperature reservoirs.

Results showed that, for the case studied here, ignoring the dissolution of CO_2 in the aqueous phase will not affect estimations of oil recovery and CO_2 sequestered volume. However, in order to know how sequestered CO_2 is distributed between different phases, including that option in the simulation is preferable.

Although 1D models showed promising results, the 3D model results showed that NGL enrichment decreased sequestered CO_2 volume without significantly increasing incremental oil recovery.

Effects of WAG ratio and slug size were minimal on oil recovery results. Sequestered CO_2 volume, however, slightly increased with decreasing slug sizes. The result indicated that the injecting CO_2 WAG in different WAG ratios and slug sizes does not affect the final oil recovery and sequestered CO_2 volume.

5.2 Recommendations

These modeling results were constrained by lack of accurate relative permeability data. Relative permeability data used in this study came from an old data set provided by the reservoir operator. To improve simulation results, it is recommended that new coreflooding experiments be conducted to obtain all relative permeability parameters, including the second HC liquid phase, for displacement of West Sak oil by CO_2.

When West Sak oil was displaced by CO_2, C1 vaporized into a separate gas phase and the CO_2 condensed into the oil phase simultaneously. To evaluate the accuracy of simulation results, a slim tube experiment and analysis of the effluent content versus time is recommended.

When CO_2 is injected into viscous and heavy reservoirs, there is a possibility of asphaltene precipitation due to changes in oil composition. In this study, the possibility and effect of asphaltene precipitation were ignored due to a lack of PVT experimental data. It is recommended to experimentally examine the possibility of asphaltene precipitation. The results can then be used to more rigorously tune the EOS. Another

simulation study could be conducted to evaluate the effect of asphaltene precipitation on oil recovery and sequestered CO_2 volume.

Only one realization of reservoir heterogeneity was used in this study. It is recommended to evaluate the effect of different heterogeneity realizations on the oil recovery and sequestered CO_2 volume.

The Schrader Bluff reservoir has similar characteristics with West Sak reservoir. It is recommended to use a similar approach taken here to evaluate the oil recovery and sequestered CO_2 volume in the Schrader Bluff reservoir.

References

Al-Meshari, A.A. and McCain, W.D., 2005. New Strategic Method to Tune Equation-of-State for Compositional Simulation, SPE Technical Symposium of Saudi Arabia Section, SPE 106332-MS. Dhahran, Saudi Arabia.

AOGCC Pool Statistics, 2004. http://doa.alaska.gov/ogc/annual/annindex.html.

Bachu, S., 2000. Sequestration of CO2 in Geological Media: Criteria and Approach for Site Selection in Response to Climate Change. Energy Conversion and Management, 41(9): 953–970.

Bakshi, A.K., 1991. Computer Modeling of CO2 Stimulation in the West Sak Reservoir, University of Alaska Fairbanks, MS Thesis.

Beeson, D.M. and Ortloff, G.D., 1959. Laboratory Investigation of the Water-Driven Carbon Dioxide Process for Oil Recovery. Journal of Petroleum Technology, 11(4): 63–66.

Benson, S.M., 2006. Benson Lab. Department of Energy Resources Engineering,Stanford University, http://pangea.stanford.edu/research/bensonlab/relperm/index.html.

Bernard, G.C., Holm, L.W. and Harvey, C.P., 1980. Use of Surfactant to Reduce CO2 Mobility in Oil Displacement. Society of Petroleum Engineers Journal, 20(4): 281–292.

Blackwell, R.J., Terry, W.M., Rayne, J.R., Lindley, D.C. and Henderson, J.R., 1960. Recovery of Oil by Displacements With Water-Solvent Mixtures. Petroleum Transactions, 219: 293–300.

Brock, W.R. and Bryan, L.A., 1989. Summary Results of CO2 EOR Field Tests, 1972–1987, Low Permeability Reservoirs Symposium, SPE 18977-MS. Denver, Colorado.

Caudle, B.H. and Dyes, A.B., 1958. Improving Miscible Displacement by Gas-Water Injection, 32nd Annual Fall Meeting of Society of Petroleum Engineers, SPE 911-G. Dallas, Texas.

Chang, Y.B., 1990. Development and Application of an Equation of State Compositional Simulator, University of Texas at Austin, PhD Dissertation.

Chang, Y.B., Coats, B.K. and Nolen, J.S., 1998. A Compositional Model for CO2 Floods Including CO2 Solubility in Water. SPE Reservoir Evaluation & Engineering, 1(2): 155–160.

Chung, F.T.H., Jones, R.A. and Burchfield, T.E., 1988. Recovery of Viscous Oil Under High Pressure by CO2 Displacement: A Laboratory Study, International Meeting on Petroleum Engineering, SPE 17588-MS. Tianjin, China.

CO2CRC Images and Videos. http://www.co2crc.com.au/imagelibrary2/general.html (accessed September 2012)

DOE/EIA, 2012. Annual Energy Outlook 2012 with Projections to 2035.

Dria, D.E., Pope, G.A. and Sepehrnoori, K. 1993. Three-Phase Gas/Oil/Brine Relative Permeabilities Measured Under CO2 Flooding Conditions. SPE Res Eng 8 (02): 143-150.

EIA, 2012a. Annual Energy Review 2011, U.S. Energy Information Administration.

EIA, 2012b. International Energy Outlook 2011, U.S. Energy Information Administration.

Enick, R.M. and Klara, S.M., 1992. Effects of CO2 Solubility in Brine on the Compositional Simulation Of CO2 Floods. SPE Reservoir Engineering, 7(2): 253–258.

EPA, 2012. Inventory of U.S. Greenhouse Gas Emissions and Sinks: 1990–2010, U.S. Environmental Protection Agency.

Gaspar, A.T.F., Suslick, S.B., Ferreira, D.F. and Lima, G.A.C., 2005. Enhanced Oil Recovery With CO2 Sequestration: A Feasibility Study of A Brazilian Mature Oil Field.

Goodrich, J.H., 1980. Review and Analysis of Past and Ongoing Carbon Dioxide Injection Field Tests, SPE/DOE Enhanced Oil Recovery Symposium, SPE 8832-MS. Tulsa, Oklahoma.

Guler, B., Wang, P., Delshad, M., Pope, G.A. and Sepehrnoori, K., 2001. Three- and Four-Phase Flow Compositional Simulations of CO2/NGL EOR, SPE Annual Technical Conference and Exhibition, SPE 71485-MS. New Orleans, Louisiana.

Henry, R.L. and Metcalfe, R.S., 1983. Multiple-Phase Generation During Carbon Dioxide Flooding. Society of Petroleum Engineers Journal, 23(4): 595–601.

Holm, L.W., 1970. Foam Injection Test in the Siggins Field, Illinois. Journal of Petroleum Technology, 22(12): 1499–1506.

Holm, L.W., 1976. Status of CO2 and Hydrocarbon Miscible Oil Recovery Methods. Journal of Petroleum Technology, 28(1): 76–84.

Hutchinson Jr, C. and Braun, P.H., 1961. Phase relations of miscible displacement in oil recovery. AIChE Journal, 7(1): 64–72.

IEA, 2002. Ocean Storage of CO2, IEA Greenhouse Gas R&D Programme.

Khan, S.A., Pope, G.A. and Sepehrnoori, K., 1992. Fluid Characterization of Three-Phase CO2/Oil Mixtures, SPE/DOE Enhanced Oil Recovery Symposium, SPE 24130-MS. Tulsa, Oklahoma.

Khataniar, S., Kamath, V.A., Patil, S.L., Chandra, S. and Inaganti, M.S., 1999. CO2 and Miscible Gas Injection for Enhanced Recovery of Schrader Bluff Heavy Oil, International Thermal Operations/Heavy Oil Symposium, SPE 54085-MS. Bakersfield, California.

Lim, M.T., Khan, S.A., Sepehrnoori, K. and Pope, G.A., 1992. Simulation of Carbon Dioxide Flooding Using Horizontal Wells, SPE Annual Technical Conference and Exhibition, SPE 24929-MS. Washington, D.C.

Lohrenz, J., Bray, B.G. and Clark, C.R., 1964. Calculating Viscosities of Reservoir Fluids From Their Compositions. Journal of Petroleum Technology, 16(10): 1171–1176.

Lu, Y., 1994. Compositional simulation of CO_2 displacement in the West Sak reservoir University of Alaska Fairbanks, MS Thesis.

McGuire, P.L. and Moritz Jr., A.L., 1992. Compositional Simulation and Performance Analysis of the Prudhoe Bay Miscible Gas Project. SPE Reservoir Engineering, 7(3): 329–334.

McGuire, P.L., Redman, R.S., Jhaveri, B.S., Yancey, K.E. and Ning, S.X., 2005. Viscosity Reduction WAG: An Effective EOR Process for North Slope Viscous Oils, SPE Western Regional Meeting, SPE 93914-MS. Irvine, California.

McKean, T.A.M., Thomas, A.H., Chesher, J.R. and Weggeland, M.C., 1999. Schrader Bluff CO2 EOR Evaluation, SPE Western Regional Meeting, SPE 54619-MS. Anchorage, Alaska.

Metcalfe, R.S. and Yarborough, L., 1979. The Effect of Phase Equilibria on the CO2 Displacement Mechanism. Society of Petroleum Engineers Journal, 19(4): 242–252.

Morye, G.G., 2007. Equation of state model development and compositional simulation of enhanced oil recovery using gas injection for the West Sak heavy oil University of Alaska Fairbanks, MS Thesis.

National Institute of Standards and Technology Standard Reference Database. Thermophysical Properties of Fluid Systems.http://webbook.nist.gov/chemistry/fluid/ (accessed 23 July 2011)

Ning, S.X., Jhaveri, B.S., Jia, N., Chambers, B. and Gao, J., 2011. Viscosity Reduction EOR with CO2 & Enriched CO2 to Improve Recovery of Alaska North Slope Viscous Oils, SPE Western North American Region Meeting, SPE 144358-MS. Anchorage, Alaska, USA.

Nourpour Aghbash, V. and Ahmadi, M., 2012. Evaluation of CO2-EOR and Sequestration in Alaska West Sak Reservoir Using Four-Phase Simulation Model, SPE Western Regional Meeting, SPE 153920-MS. Bakersfield, California, USA.

Okuno, R., Johns, R.T. and Sepehrnoori, K., 2011. Mechanisms for High Displacement Efficiency of Low-Temperature CO2 Floods. SPE Journal, 16(4): pp. 751–767.

Orr, F.M., 2004. Storage of Carbon Dioxide in Geologic Formations. Journal of Petroleum Technology, 56(9): 90–97.

Orr, F.M., Yu, A.D. and Lien, C.L., 1981. Phase Behavior of CO2 and Crude Oil in Low-Temperature Reservoirs. Society of Petroleum Engineers Journal, 21(4): 480–492.

Panda, M.N., Zhang, M., Ogbe, D.O., Kamath, V.A. and Sharma, G.D., 1989. Reservoir Description of West Sak Sands Using Well Logs, SPE California Regional Meeting, 18759-MS. Bakersfield, California.

Peng, D.Y. and Robinson, D.B., 1976. A New Two-Constant Equation of State. Industrial & Engineering Chemistry Fundamentals, 15(1): 59–64.

Rao, D., 2001. Gas Injection EOR-A new meaning in the new millennium. Journal of Canadian Petroleum Technology, 40(2).

Sahin, S., Kalfa, U. and Celebioglu, D., 2008. Bati Raman Field Immiscible CO2 Application-Status Quo and Future Plans. SPE Reservoir Evaluation & Engineering, 11(4): pp. 778-791.

Saner, W.B. and Patton, J.T., 1986. CO2 Recovery of Heavy Oil: Wilmington Field Test. Journal of Petroleum Technology, 38(7): 769-776.

Sharma, G., 1990. Development of Effective Gas Solvents Including Carbon Dioxide for the Improved Recovery of West Sak Oil, University of Alaska Fairbanks, Fairbanks, AK.

Shelton, J.L. and Yarborough, L., 1977. Multiple Phase Behavior in Porous Media During CO2 or Rich-Gas Flooding. Journal of Petroleum Technology, 29(9): 1171–1178.

Simon, R. and Graue, D.J., 1965. Generalized Correlations for Predicting Solubility, Swelling and Viscosity Behavior of CO2-Crude Oil Systems. Journal of Petroleum Technology, 17(1): 102–106.

Stalkup Jr., F.I., 1983. Status of Miscible Displacement. Journal of Petroleum Technology, 35(4): 815–826.

Staub, J., Rasmussen, B.D., and Robinson, M., 2004. CO2 as Refrigerant: The Transcritical Cycle. http://www.achrnews.com/articles/co2-as-refrigerant-the-transcritical-cycle (accessed July,2012)

Stone, H.L. and Crump, J.S., 1956. The Effect of Gas Composition Upon Oil Recovery by Gas Drive. Petroleum Transactions, 207: 105–110.

Targac, G.W., Redman, R.S., Davis, E.R. et al., 2005. Unlocking the Value in West Sak Heavy Oil, SPE/PS-CIM/CHOA International Thermal Operations and Heavy Oil Symposium, SPE 97856-MS. Calgary, Alberta, Canada.

Turek, E.A., Metcalfs, R.S., Yarborough, L. and Robinson Jr., R.L., 1984. Phase Equilibria in CO2 - Multicomponent Hydrocarbon Systems: Experimental Data and an Improved Prediction Technique. Society of Petroleum Engineers Journal, 24(3): 308–324.

Twu, C.H., 1984. An Internally Consistent Correlation for Predicting the Critical Properties and Molecular Weights of Petroleum and Coal-Tar Liquids. Fluid Phase Equilibria, 16(2): 137–150.

Wang, G.C. and Locke, D.C., 1980. A Laboratory Study of the Effects of CO2 Injection Sequence on Tertiary Oil Recovery. Society of Petroleum Engineers Journal, 20(4): 278–280.

Wang, P. and Pope, G.A., 2001. Proper Use of Equations of State for Compositional Reservoir Simulation. Journal of Petroleum Technology, 53(7): 74–81.

Wang, X. and Strycker, A., 2000. Evaluation of CO2 Injection with Three Hydrocarbon Phases, International Oil and Gas Conference and Exhibition in China, SPE 64723-MS. Beijing, China.

Well File Image Database - Alaska Oil and Gas Conservation Commission. http://aogweb.state.ak.us/weblink7/Browse.aspx (accessed 19 June 2011)

Werner, M., 1987. Tertiary and Upper Cretaceous Heavy Oil Sands, Kuparuk River Unit Area, Alaskan North Slope. Exploration for Heavy Crude Oil and Natural Bitumen: American Association of Petroleum Geologists Studies in Geology(25): 537–548.

Whorton, L.P. and Kieschnick, W.F., 1950. A preliminary Report on Oil Recovery by High-Pressure Gas Injection. American Petroleum Institute.

Yan, W. and Stenby, E.H., 2009. The Influence of CO2 Solubility in Brine on CO2 Flooding Simulation, SPE Annual Technical Conference and Exhibition, SPE 124628-MS. New Orleans, Louisiana.

Yan, W. and Stenby, E.H., 2010. The Influence of CO2 Solubility in Brine on Simulation of CO2 Injection into Water Flooded Reservoir and CO2 WAG, SPE EUROPEC/EAGE Annual Conference and Exhibition, SPE 131094-MS. Barcelona, Spain.

Zick, A.A., 1986. A Combined Condensing/Vaporizing Mechanism in the Displacement of Oil by Enriched Gases, SPE Annual Technical Conference and Exhibition, SPE 15493-MS. New Orleans, Louisiana.

Appendix

The UTCOMP simulator was used in this study. UTCOMP requires an input data file for the non-restart runs and an additional restart file for the restart runs. The data file is named "INPUT.DAT". The executable file reads the input data file and generates the output files. The UTCOMP user guide provides a comprehensive description of the input and output files. Following is a summarized list and a brief description for some of the output files:

TEST.PRF: This is a profile data file for the 1D runs. The file includes time, pressure, saturations, overall composition, phase compositions, relative permeabilities, viscosities, densities, etc for each grid block.

TEST.HIS: This is a well-history data file. It includes time, cumulative hydrocarbon component production/injection, cumulative water production/injection, total surface production/injection rates, oil recovery, GOR, WOR, effluent concentration, etc.

TEST.CON: This is a contour data file for 2D and 3D runs. Similar to "TEST.PRF" data file, it includes time, pressure, saturations, overall composition, phase compositions, relative permeabilities, viscosities, densities, etc for each grid block.

Dr. Sepehrnoori is the head of UTCOMP development team and can be reached at kamys@mail.utexas.edu.